The Thesis Committee for Jessica Bauman
Certifies that this is the approved version of the following thesis:

Alterations in Resting-State Functional Connectivity in Primary Progressive Aphasia

APPROVED BY
SUPERVISING COMMITTEE:

Supervisor: _____
Maya Henry

_____
Bharath Chandrasekaran

Alterations in Resting-State Functional Connectivity in Primary Progressive Aphasia

by

Jessica Bauman, B.S.

Thesis

Presented to the Faculty of the Graduate School of

The University of Texas at Austin

in Partial Fulfillment

of the Requirements

for the Degree of

Master of Arts

The University of Texas at Austin

May, 2016

Dedication

I would like to dedicate my thesis to my parents, who have supported me throughout my life and helped me get to where I am now. I would also like to thank my amazing boyfriend, Sami. For all the late nights and all-nighters, pep-talk sticky notes and constant support, I thank you from the bottom of my heart. I could not have done this without you.

Acknowledgements

I would like to thank and acknowledge Dr. Henry for her immense patience, mentorship and immesurable contribution to this project. I would also like to acknowledge my undergraduate research assistant Morgan, who has put countless hours into research tasks both big and small. I am proud to call her my friend, as well as colleague, and thank her for her friendship and hard work. I would also like to acknowledge Stephanie and Mithra for their contribution and support throughout this process. Troubleshooting computer errors, BPM issues and difficult data analysis has been a group effort. A big thank you to my entire team for making this thesis a finished product.

Abstract

Alterations in Resting-State Functional Connectivity in Primary Progressive Aphasia

Jessica Bauman, M.A.

The University of Texas at Austin, 2016

Supervisor: Maya Henry

Primary progressive aphasia (PPA) is a neurodegenerative disorder affecting speech and language, which presents as three clinical variants: nonfluent PPA (nfvPPA), logopenic PPA (lvPPA), and semantic PPA (svPPA). PPA selectively targets dorsal left hemisphere regions involved in articulatory and phonological processing in nfvPPA and lvPPA and ventral lexical-semantic regions in svPPA. The aim of the current study was to investigate alterations in resting-state functional connectivity (RSFC) within key areas of dorsal and ventral language pathways in PPA relative to controls. We addressed this aim using a region of interest seed-based approach, with left hemisphere seeds located in: (1) the inferior frontal gyrus (IFG), (2) an area within the posterior Sylvian fissure at the temporo-parietal junction (SPT), and (3) the anterior temporal lobe (ATL). Participants included 22 patients with lvPPA, 32 patients with nfvPPA, 25 patients with svPPA and

39 healthy controls. Voxel-based morphometry (VBM) analysis was performed in order to identify areas of significant regional atrophy in patients. Subsequently, functional language networks were defined in healthy controls and in each patient group, and significant group differences in resting-state functional connectivity were determined after correction for gray matter volume. Results revealed reductions in connectivity among all patient groups for all seeded networks. Different patterns of RSFC alteration were also seen within each patient group. These findings provide evidence of selective functional and structural alterations in each of the clinical variants of PPA.

Table of Contents

List of Tables

List of Figures

I. Introduction

Primary progressive aphasia (PPA) is a neurodegenerative disorder characterized by a slow decline in speech-language abilities in the relative absence of other cognitive or behavioral impairment (Gorno-Tempini, et al., 2004, 2011). The brain undergoes relatively focal atrophy in key areas of the primarily left-lateralized language system, disrupting phonological, semantic, syntactic, and motoric speech and language networks. Three variants of PPA exist: non-fluent variant PPA (nfvPPA), logopenic variant PPA (lvPPA), and semantic variant PPA (svPPA), as determined by speech and language characteristics. Patients with nfvPPA demonstrate speech production impairment related to agrammatism and apraxia of speech. Atrophy is predominantly in the left inferior frontal, insular, and premotor cortex (Gorno-Tempini et al., 2004; Rohrer et al., 2009; Wilson, Galantucci, Tartaglia, & Gorno-Tempini, 2012). Other areas in the frontal lobe, as well as the temporal lobe, anterior parietal lobe, and caudate nucleus, may be affected as the disease progresses (Roglaski et al., 2011). Those with lvPPA demonstrate poor repetition of sentences, phonemic paraphasias, and anomia with preserved word comprehension (Gorno-Tempini et al., 2004, 2011). Atrophy is typically observed in perisylvian regions thought to support phonological processing, including the left posterior temporal and inferior parietal lobes, sometimes spreading into the posterior frontal lobe (Lehmann et al., 2013; Tomasi & Volkow, 2012). Pathologically, lvPPA is a subtype of Alzheimer's disease. As such, it may ultimately present with similar/overlapping features but is classified based on early and primary deficits of

language. Unlike lvPPA, semantic variant PPA is characterized by a progressive deterioration of conceptual knowledge, and patients present with fluent but anomic spontaneous speech (Gorno-Tempini et al., 2011; Hodges & Patterson, 2007). Phonology in svPPA is relatively spared, and syntax, prosody, and articulation remain intact (Gorno-Tempini et al., 2011). Atrophy is typically seen bilaterally in the ventral and lateral portions of the anterior temporal lobe (Hodges & Patterson, 2007; Mummery et al., 2000), regions thought to be "hubs" for semantic processing (Guo et al., 2013; Hurley, Bonakdarpour, Wang & Mesulam, 2015). Both semantic variant PPA and nfvPPA are considered to be types of frontotemporal dementia (FTD), differentially diagnosed relative to the behavioral variant of FTD by a lack of behavioral abnormalities and primary impairment of speech and language only.

1.1. Dorsal and Ventral Language Streams

Current models of the cognitive neuroanatomy of language propose two pathways by which speech and language are processed in the brain: a dorsal articulatory-phonological pathway and a ventral lexical-semantic pathway (Hickok & Poeppel, 2004: Hickok, 2012, 2014; Saur et al., 2008; Ueno, Saito, Rogers, & Lambon Ralph, 2011). The dorsal articulatory-phonological pathway, involving left temporoparietal and frontal perisylvian structures, is thought to be involved in mapping sound and phonological representations to articulatory representations. The ventral lexical-semantic pathway, involving the left middle and inferior temporal lobes, maps sound to meaning (Henry et al., 2016; Hickok, 2014). Within this model, a region within the Sylvian fissure at the

parietal-temporal boundary (area SPT) interfaces with both the ventral and dorsal language streams as a sensorimotor interface (Hickok, Okada, & Serences, 2009; Rauschecker & Scott, 2009). The Hickok dorsal-ventral model of speech and language processing does not address phonological short-term memory or manipulation, per se; however, cooperative and interactive participation of dorsal left frontal and temporoparietal regions is hypothesized for manipulation and maintenance of phonological information (Henry et al., 2016). Functional neuroimaging research and lesion studies support this model of integrated dorsal fronto-parietal and ventral temporo-parietal language function (Buhsbaum & D'Esposito, 2008; Champod & Petrides, 2010; Kümmerer et al., 2013; Peschke, Ziegler, Eisenberger, & Baumgaertner, 2012; Rauschecker & Scott, 2009; Vigneau et al., 2006). Behavioral deficits for nfvPPA/lvPPA and svPPA coincide with proposed dorsal articulatory-phonological and ventral semantic language pathway functions, respectively (Gorno-Tempini et al., 2011). Given that peak atrophy regions for nfvPPA, lvPPA and svPPA overlap with key nodes within dorsal and ventral language streams, i.e. inferior frontal gyrus (IFG), area SPT, and the anterior temporal lobe (ATL), respectively, the dorsal-ventral model for speech and language processing becomes especially salient for understanding selective language breakdown within PPA. PPA is understood to be a disorder of network-based degeneration (Seeley, Crawford, Zhou, Miller, & Greiciuss, 2009). The neuroanatomy of the disease is not dictated by vascular factors (as in aphasia caused by stroke), but by connectivity underlying specific speech-language networks (Seeley et al., 2009). As such, PPA offers

a unique vantage from which to explore language function and selective decline within a dual-route language perspective.

1.2. NEUROIMAGING IN PPA

The close relationship between atrophy and speech and language deficits makes neuroimaging a valuable tool for understanding the neural bases of communication and clinical progression of speech-language deficits in patients. A variety of neuroimaging techniques have emerged in recent years to capture network degeneration of gray matter and white matter on a structural level, such as voxel-based morphometry (VBM; Gorno-Tempini et al., 2004; Mummery et al., 2000; Peelle et al., 2008; Sonty et al., 2003) and diffusion tensor imaging (DTI; Acosta-Cabronero et al., 2011; Galantucci et al; Mahoney et al., 2013; Schwindt et al., 2013). Neuroimaging techniques have also emerged to measure changes in functional network organization and connectivity within the brain. Resting-state functional connectivity (RSFC) magnetic resonance imaging is an imaging technique that captures and maps the functional connectivity of intrinsic networks within the brain, making it an ideal technique for studying PPA, as widespread degeneration of the language network is seen in PPA patients over time (Seeley et al., 2009).

Resting-state fMRI is a task-free imaging method that measures spontaneous low frequency (<0.08-0.1 Hz) fluctuations in the blood oxygen level dependent (BOLD) signal during rest (Pievani, de Haan, Wu, Seeley, & Frisoni, 2011). The BOLD signal relies on changes in the ratio between oxyhemoglobin and deoxyhemoglobin after neuronal activity to provide an indirect measure of neuronal function on a timescale of

seconds. The functional marker of BOLD signal temporal correlations between spatially distinct regions is referred to as functional connectivity and represents an marker of spontaneous activity within spatially distinct, but functionally related, cortical regions (Beckmann, DeLuca, Devlin, & Smith, 2005).

Several methods have emerged for analyzing RSFC data, including independent component analysis (ICA), graph theory seed-based analysis, magnetoencephalographic imaging (MEGI) and region-of-interest (ROI) seed-based analysis. ICA and graph theory are mathematically derived and rely on statistical and small world topology to draw conclusions about intrinsic connectivity. ICA identifies statistically independent components of the brain's temporal BOLD signal and uses resulting components to isolate spatially distinct resting-state networks (Lee, Smyser, & Shimony, 2013; Rosazza, Minati, Ghielmetti, Mandelli, & Bruzzone, 2012). Graph theory, in contrast, views correlations between voxels as a collection of graphical nodes connected by edges. Such a model allows the computation of connectional characteristics of the network such as characteristic path length, clustering coefficients, and measures of global connectedness. Unlike an ICA or graph theory approach, MEGI records fluctuations in RSFC of alpha-band activity and applies source reconstruction algorithms to overlay cortical oscillatory activity onto structural brain images, thereby performing an unbiased search for resting-state networks (Ranasinghe et al., 2014). Finally, ROI seed-based analysis of RSFC data correlates the average BOLD time course of voxels within specific regions of interest in the brain (seed ROIs) to the time courses of all other voxels in a second ROI or the entire brain. Seed-based approaches rely on selection of ROIs *a priori*, creating small statistical

bias in the connectivity found between areas of the brain; however, seed-based approaches have been proven to be relatively robust and produce comparable results to methods such as ICA, making them an ideal candidate for examining connectivity of already established areas of function, such as in the language network (Lee et al., 2013).

1.3. Network Characteristics of PPA

Alterations in RSFC within a variety of networks have been identified in PPA, including the learning and memory networks (La Joie et al., 2014; Ranasinghe et al., 2014; Whitwell et al., 2015), salience network (Day et al., 2013; Farb et al., 2013; Lehmann et al., 2013; Zhou et al., 2010), default mode network (Lehmann et al., 2013, 2015; Seeley et al., 2009; Zhou, et al., 2010), language networks (Agosta et al., 2013; Guo et al., 2013; Lehmann et al., 2013, 2015; Ranasinghe et al., 2014; Seeley et al., 2009; Whitwell et al., 2015; Zhou, Gennatas, Kramer, Miller, & Seeley, 2012), visuospatial networks (Agosta et al., 2013; Lehmann et al., 2015; Ranasinghe et al., 2014), and executive-control networks (Farb et al., 2013; Lehmann et al., 2013, 2015; Ranasinghe et al., 2014). Although PPA is exclusively defined by degeneration of language, surprisingly little research exists on alterations in RSFC for the language networks within PPA patients. Of the existing literature, even fewer studies analyze resting-state network changes by variant. To the author's knowledge, at this date no study exists that compares the resting-state functional connectivity of language networks in and between lvPPA, nfvPPA, and svPPA relative to healthy controls. Such a comparison can provide unique

and valuable clinical insight for differential diagnosis of PPA and potentially serve as a predictive marker for responsiveness to behavioral treatment.

1.4. Alterations in nfvPPA Resting-State Functional Connectivity

Of all three variants of PPA, nfvPPA has the least research on RSFC patterns within the language network. In a study designed to assess alterations in connectivity between presymptomatic and symptomatic carriers of the genetic Granulin Thr272fs (GRN+) mutation for frontotemporal dementia (FTD), Premi et al. (2014) demonstrated asymmetric fronto-parieto-temporal connectivity in a mixed group of nfvPPA, behavioral variant FTD (bvFTD), and asymptomatic carriers of the GRN+ mutated gene (all in one group; FTD-GRN+) compared to healthy controls. FTD-GRN+ participants showed a reduced regional homogeneity index (e.g. degree of regional fMRI time course synchronization) bilaterally in the inferior parietal and frontal lobes, including the left IFG, as well as in the left posterior cingulate cortex. An increase in frontal functional connectivity for FTD-GRN+ was observed, along with recruitment of the cerebellar lobes. Such data could suggest reduced efficiency in the inferior frontal lobes as a result of poor synchronization or general misfiring. As asymptomatic carriers of the GRN+ gene were included in the FTD-GRN+ group, it is unclear to what extent results accurately reflect alterations in brain connectivity by subgroup (e.g. for nfvPPA).

1.5. ALTERATIONS IN AD AND LVPPA RESTING-STATE FUNCTIONAL CONNECTIVITY

Several researchers have investigated the language networks using RSFC analysis in Alzheimer's disease (AD) patients. Lehmann et al., (2013) conducted an ROI seed-based analysis in healthy controls using coordinates garnered from atrophy peaks in early-onset AD (EOAD), lvPPA, and posterior cortical atrophy (PCA) patients. Seeds utilized included those within shared areas of atrophy and within non-overlapping areas of atrophy for all AD variants. Resulting RSFC maps produced from each variant's distinct ROI mirrored the networks associated with the predominant cognitive deficit seen in each syndrome. Specifically, within healthy controls, the EOAD ROI-seeded RSFC map had the strongest goodness-of-fit (GOF) with the salience/executive control networks, while the lvPPA ROI-seeded RSFC map most closely matched a language network template and PCA ROI-seeded RSFC map most closely fit the higher visual network.[1] Lehmann and colleagues expanded this work in 2015 to include both controls and patients (EOAD, lvPPA, and PCA) in a ROI seed-based RSFC analysis. ROI seeds were explicitely defined from coordinates representing areas of maximum atrophy in each patient population. Connectivity for lvPPA and EOAD was particularly reduced in the anterior regions of the parietal lobe, whereas connectivity in the prefrontal cortex of the anterior default mode network was higher in lvPPA and PCA compared to controls and EOAD. Using GOF analyses, resulting networks were then compared to default mode, executive-control, language, and higher visual network templates. Consistent with

[1] Network templates utilized in the goodness-of-fit analyses for the executive control, salience, default mode, language and higher visual function networks were not explicitely defined in either Lehmann et al., 2013 or 2015.

predictions based on the previous study, EOAD, lvPPA, and PCA groups had reductions in the RSFC anterior left and right executive-control network, language network, and higher visual network; however, differences between network connectivity scores were not significant between variant AD groups, suggesting that changes across AD clinical presentations may be a spectrum.

Similar to the Lehmann studies, but using ICA, Whitwell et al., (2015) found lower connectivity in the left temporal language network and inferior parietal and prefrontal regions of the left working memory network in Alzheimer's disease patients compared to controls.[2] Patterns of network dysfunction differed across groups, with lvPPA demonstrating significant disruptions in the language and left working memory networks as compared to controls. Such disruptions correlated with behavioral data in lvPPA, including poor performance on naming and letter fluency task as well as sentence repetition and increased prevalence of phonemic paraphasias.

Ranasinghe et al., (2014) utilized MEGI to identify regional resting-state networks in AD and correlate results to disease severity and cognitive performance in EOAD (amnestic/dysexecutive), lvPPA, PCA, and mild cognitive impairment (MCI). lvPPA patients scored low in lexical fluency and presented with reduced functional connectivity in the left dorsolateral prefrontal cortex. PCA patients, in contrast, generally scored high on lexical fluency with increased functional connectivity in the region. Interestingly, Ranasinghe et al. found reduced neural connectivity of the right posterior

[2] The language, left and right working memory and ventral default mode networks were initially defined using ICA in a separate cohort of healthy controls. They were assigned a network name per a functional meta-analysis by Jones et al., 2012.

perisylvian region and left middle frontal cortex in all AD population groups, which correlated with the overall degree of disease severity. Both Ranasinghe et al. and Whitwell et al. confirmed Lehmann's original findings, which demonstrated decreased functional connectivity in the left dorsolateral prefrontal cortex. However, Whitwell et al. and Lehmann et al. showed additional reductions in connectivity within the left perisylvian region. More research is needed to determine whether reductions in functional connectivity for lvPPA are greatest in the left dorsolateral prefrontal cortex or perisylvian region, where atrophy is frequently greatest.

1.6. Alterations in svPPA Resting-State Connectivity

As svPPA is considered a form of FTD, most research on resting-state functional connectivity in svPPA is conducted within the context of FTD. Current svPPA resting-state research focuses on the salience network, default mode network, and executive-control network (Farb et al., 2013; Filippi et al., 2012; Irish, Hodges, & Piguet, 2013; Rohrer et al., 2013; Whitwell et al., 2011b; Zhou et al., 2010). Relative to language, fewer studies exist; however, recent studies have began to examine the effects of svPPA on RSFC within the language network. In 2013, Guo et al. compared patterns of functional connectivity based on bilateral anterior temporal lobe seeds between svPPA patients and healthy controls. Resting-state connectivity of the ATL with numerous modality-selective regions was reduced in svPPA relative to healthy controls. Specifically, the ATL had altered connectivity to primary sensory and motor regions, modality-selective and heteromodal association cortices, as well as subcortical regions.

Alterations in connectivity correlated with scores on semantic tasks in svPPA patients. The authors interpreted robust intrinsic connections between the ATLs and a host of primary and modality-selective upstream regions as support for the claim that the ATL serves as a semantic "hub" within an integrated semantic network (Gou et al., 2013; Patterson, Nestor, & Rogers, 2007).

Agosta et al., (2013) further examined connectivity of the language network in svPPA using graph theory analysis to isolate nodal vulnerabilities of functional networks in svPPA versus healthy controls. The svPPA group demonstrated sparing of the parietal network nodes, but a significantly reduced number of graphical nodes in the left and right temporal lobes and the occipital lobe. Interestingly, the left ITG was identified as a hub in controls, but not svPPA, and no occipital hubs were identified in svPPA. Hubs indicate areas of high information exchange. Global efficiency, characteristic path length, and assortativity (i.e. high degree nodes are connected to other high degree nodes, and low degree nodes connected to low degree nodes) were all found to be poorer in svPPA as compared to controls. Results suggest a loss of efficiency in information exchange between local and distant regions. In contrast, the superior temporal gyrus, middle frontal gyrus and thalamus bilaterally, right inferior frontal gyrus, and left precentral gyrus and supplementary motor area were hubs in svPPA only, and may represent compensatory areas of activation. Decreased temporal and occipital connectivity are consistent with results from Guo et al., (2013), as behavioral deficits such as visual feature and object knowledge loss are frequently seen in svPPA. Such behavioral characteristics may possibly be a result of reduced occipital and temporal connectivity.

Although not directly examining RSFC within patients, in a unique study encompassing all three subtypes of PPA, as well as bvFTD and corticobasal syndrome (CBS), Seeley et al., (2009) utilized coordinates of peak atrophy within each patient group as a seed for an ICA-based RSFC analysis in healthy controls and compared it to gray matter covariance patterns using the same seed. Resulting RSFC networks were then matched via goodness-of-fit analysis to source atrophy maps in order to identify which networks were targeted by each neurodegenerative disease. Results showed distributed dissociable network maps in healthy controls for seeds from bvFTD, svPPA, AD (including lvPPA), CBS, and nfvPPA, with converging structural covariance for each respective seed. Furthermore, RSFC networks within healthy controls seeded from areas of patient atrophy mirrored the actual atrophy patterns seen in patient groups, demonstrating that specific RSFC networks are targeted by neurodegenerative diseases in patterns similar to both the intrinsic structural covariance and gray matter loss. Seeley interpreted these findings as evidence for the "network degeneration hypothesis," namely: networks and gray matter volumes uniquely codegenerate according to disease-specific patterns predicted by the convergence of structural atrophy and functional connectivity.

Zhou et al., expanded on Seeley's results in 2012, and used graph theory to analyze how network connectivity in healthy controls can predict network vulnerability in neurodegenerative disease groups (svPPA, nfvPPA, AD, CBS, and bvFTD) on a region-by-region basis. Graph theory metrics that were examined included total flow, shortest functional path to epicenters, and clustering coefficients. These metrics were

used to evaluate four major mechanistic models for connectivity-related predictions: the nodal stress model, transneuronal spread hypothesis, trophic failure model, and shared vulnerability model. Network vulnerability was best predicted by greater total connectional flow through disease epicenter nodes, with the shortest functional path to the epicenters accounting for more atrophy variance within AD and svPPA patterns. The epicenter identified for AD was in the angular gyrus, while epicenters for disease in svPPA and nfvPPA were in the ATL and IFG, respectively. NfvPPA also had epicenters in striatal and thalamic sites with robust operculofrontal connections. Patient groups demonstrated divergent nodal disease profiles and network graphs, with the most divergent network profiles seen in AD and bvFTD. Furthermore, across all five diseases, network nodes subject to greater intranetwork total connectional flow were found to undergo greater atrophy, further supporting the transneuronal spread hypothesis.

Although Seeley et al. and Zhou et al. both examined RSFC patterns of the language network based on atrophy in PPA patient populations, data were analyzed only in healthy controls. Furthermore, lvPPA patients were not examined as a separate subset, but instead were grouped with AD patients. Both papers utilized methods that failed to directly compute and compare resting-state data within PPA groups themselves. As such, it is unknown to what extent such networks are altered in PPA as compared to controls, and further, how such alterations affect language behavior. The current study used an ROI seed-based approach to examine alterations in language network resting-state connectivity in lvPPA, svPPA, and nfvPPA as compared to controls, representing an

integral first step toward understanding the relationship between network dysfunction and language decline in primary progressive aphasia.

Our predictions were as follows:

(1) Extent and Site of Atrophy: On the basis of cortical thickness mapping and voxel-based morphometry (VBM) studies, we predicted that the nfvPPA group would have atrophy primarily in the dorsal articulatory-phonological language pathway, specifically within the insula, prefrontal cortex and motor strip (Gorno-Tempini et al., 2004; Rohrer et al., 2009; Wilson et al., 2012). Consistent with more recent literature on gray matter loss in lvPPA, we predicted that lvPPA would have atrophy in the temporoparietal perisylvian region, extending into both dorsal and ventral language pathways (Lehmann et al., 2013; Tomasi & Volkow, 2012). Finally, we predicted left-dominant bilateral temporal atrophy within the ventral lexical-semantic pathway for svPPA, consistent previous VBM studies (Hodges & Patterson, 2007; Mummery et al., 2000).

(2) Extent of RSFC Networks: Although RSFC in specific, key areas of the language network has not been investigated for all PPA variants, the literature demonstrates general group-level reductions in RSFC, as compared to controls (Agosta et al., 2013; Guo et al., 2013; Lehmann et al., 2015; Ranasinghe et al., 2014; Whitwell et al., 2015). We hypothesized that functional connectivity networks derived from IFG, SPT and ATL seeds would be less extensive in patients relative to controls and

demonstrate unique patterns of network-wide dysfunction, consistent with Guo et al., (2013), Lehmann et al., (2015), and Seeley et al., (2009).

(3) Alterations in RSFC Relative to Controls: We hypothesized that the nfvPPA group would have widespread disturbance in dorsally seeded articulatory-phonological networks (IFG and SPT seeds), which are critical for effective motor-speech and syntax. Although the current literature does not provide substantial insight into the specific nature of RSFC alterations within nfvPPA, such a prediction is consistent with corresponding behavioral language deficits seen in nfvPPA (Gorno-Tempini et al., 2011). In contrast, we hypothesized that lvPPA would show prominent left hemisphere disruption in networks derived from dorsal (e.g. SPT and IFG) seeds, with reduced but less impaired RSFC within the ventrally seeded (ATL) networks, similar to Ranasinghe et al., (2014), Whitwell et al., (2015) and Lehmann et al., (2015). Finally, for svPPA, we predicted widespread RSFC disruptions primarily in the ventrally seeded semantic network (ATL seed), with relatively intact dorsal articulatory-phonological seeded networks (e.g. IFG and SPT). Such a prediction is consistent with graph theory results from Agosta et al., (2013), demonstrating reduced graph theory nodes within bilateral temporal and occipital lobes but spared parietal regions, as well as behavioral data demonstrating impaired semantic processing but relatively

spared phonological and motor speech abilities in svPPA (Gorno-Tempini et al., 2011).

II. Methods

2.1. PARTICIPANTS

Participants in each patient group were selected from the University of California, San Francisco (UCSF) Memory and Aging Center database. 22 patients with lvPPA, 32 patients with nfvPPA, 25 patients with svPPA, and 39 age-matched healthy controls were selected. As part of their participation in a large study of focal dementias at UCSF, individuals in the patient subgroups underwent a complete clinical history, neurological examination, and a speech, language, and neuropsychological assessment, as previously described (Mandelli et al., in press; Rosen et al., 2002). Patients met current criteria for PPA diagnosis by variant, as agreed upon by a multidisciplinary team (Gorno Tempini et al., 2011; Mandelli et al., in press; Seeley et al., 2009). Informed consent was obtained from all participants or their assigned surrogate. Control participants were required to have a Clinical Dementia Rating Scale total score of 0 (*CDR*; Morris, 1993), a Mini-Mental State Examination score of 28 or higher (*MMSE*; Folstein M., Folstein S., & McHugh P., 1993), no significant history of neurological disease, and no evidence of conversion to a dementia syndrome at follow-up (when available). The study was approved by the institutional review boards at UCSF and University of Texas at Austin (UT Austin). Participant demographics are shown in Table 1.

Table 1: Participant Age, Sex, Handedness and Mini Mental State Exam Score by Group

	Age (years)	Sex (M:F)	Handedness (L:R:A)*	Mini Mental State Exam** (30)
Healthy controls (n=39)	69.67 (5.02)	16:23	7:32:0	29.66 (0.64)
nfvPPA (n=32)	67.38 (7.18) [a]	14:18	4:27:0	26.07 (4.30) [a]
lvPPA (n=22)	64.18 (8.31) [a]	9:13	6:14:1	18.81 (7.95) [a,b,d]
svPPA (n=25)	62.44 (5.88) [a,b]	13:12	1:23:1	23.88 (6.08) [a]

Means and standard deviations given for Age and Mini Mental State Exam (*MMSE*); M=male; F=female; L=left, R=right, A=ambidextrous; *indicates missing handedness data (1 nfvPPA, 1 lvPPA); **indicates missing *MMSE* data (4 controls, 2 nfvPPA, 1 lvPPA); [a] = significantly reduced relative to controls, [b] = significantly reduced relative to nfvPPA; [c] = significantly reduced relative to lvPPA; [d] = significantly reduced relative to svPPA (p<0.05).

2.2. Scan Acquisition

Structural T1 and functional resting-state images were acquired for all participants at the Neuroscience Imaging Center, at UCSF, as part of a large imaging and behavioral study of PPA/FTD on a 3T Siemens magnetic resonance imaging (MRI) scanner equipped with an eight-channel head coil.

A volumetric magnetization prepared rapid gradient echo (MPRAGE) MRI sequence was used to obtain a T1-weighted image of the entire brain in sagittal slices (160 sagittal slices; slice thickness=1 mm; field of view=256 mm^2; matrix 256X240; voxel size 1.0X1.0X1.0 mm^3; repetition time=2300 ms; echo time=2.98 ms; inversion time=900 ms; flip angle=9°). Resting-state fMRI (rsfMRI) sequences were acquired in the same session on the 3T scanner using 240 T2*-weighted echo-planar volumes with 36 anterior and posterior commissure-aligned axial slices in an interleaved order (slice thickness=3 mm with a 0.6 mm gap; field of view=230X230 mm^2; matrix size=92X92;

TR=2000 ms; TE=27 ms; flip angle=80°). Participants were instructed to rest with their eyes closed for the duration of the scan.

2.3. OVERVIEW

The aim of the current study was to investigate alterations in RSFC within key areas of the dorsal and ventral language streams in PPA relative to controls. To do so we implemented the following steps:

Step 1: Preprocess structural T1 and RSFC scans

Preprocessing was completed using Statistical Parametric Mapping (SPM) version 8 (http://www.fil.ion.ucl.ac.uk/spm/software/spm8/), FSL version 5 (http://fsl.fmrib.ox.ac.uk/fsl/fslwiki/), AFNI (http://afni.nimh.nih.gov/afni/), Numpy in Python 2.7.3., and a UCSF-developed RSFC imaging toolbox (Mandelli et al., in press).

Step 2: Selection of language network seeds

Seeds within the dorsal and ventral language streams were selected based on converging evidence from functional imaging studies of language processing in healthy controls and peak atrophy regions in each variant of PPA (see details below). Two seeds from the dorsal language stream in the inferior frontal gyrus (IFG) and posterior perisylvian region at the parietal-temporal boundary (area SPT) were chosen, representing dorsal stream nodes and atrophy peaks in nfvPPA and lvPPA respectively. The IFG is heavily implicated in syntax and articulatory-phonological processing, while area SPT is thought to be a sensorimotor interface for phonological representations of

speech (Henry et al., 2016; Hickok, 2012, 2014; Rauschecker & Scott, 2009). One seed within the ventral lexical-semantic stream was chosen in the anterior temporal lobe (ATL), representing a key region for semantics in the language network, as well as a constistently atrophic area in svPPA (Binder, Desai, Graves & Conant, 2009; Gorno-Tempini et al., 2011).

Step 3: Identify regions of significant atrophy in PPA patient groups

We computed voxel-wise gray matter loss in patients relative to healthy controls using a voxel-based morphometry toolkit (VBM8) within SPM (http://www.neuro.uni-jena.de/vbm/) to identify areas of significant gray matter atrophy.

Step 4: Delineate resting-state functional connectivity maps for seeds in each group

Anterior temporal lobe (ATL), inferior frontal gyrus (IFG), and temporoparietal (SPT) coordinates were used as the centers of spherical seed ROIs (4mm radius) to define functional language networks in healthy controls, lvPPA, nfvPPA, and svPPA, respectively (see Figure 1).

Step 5: Determine significant group differences in resting-state functional connectivity

We compared patient seed maps to control maps while controlling for gray matter volume using analysis of covariance (ANCOVA) implemented in the Biological Parametric Mapping (BPM) toolbox (http://www.nitrc.org/projects/rbpm) for SPM.

2.4. DETAILED PROCEDURES

2.4.1. Step 1— Preprocess structural T1 and resting-state images

Structural T1 scans were segmented into gray matter, white matter, and cerebrospinal fluid using VBM for SPM within Matlab version 2010 (The MathWorks, Inc.), according to previously documented procedures (Henry et al., 2016). RSFC scans were preprocessed using a UCSF RSFC toolbox, as described in Mandelli et al., in press. T1 structural images were segmented and bias-corrected, then registered to Montreal Neurological Institute (MNI) space through an affine and a non-linear deformation. The non-linear deformation parameters were calculated with the high dimensional diffeomorphic anatomical registration through exponentiated lie (DARTEL) algorithm and the predefined templates within the SPM DARTEL toolbox (Ashburner, 2007). The VBM analysis was conducted using modulated grey matter images, with voxel values multiplied by Jacobian determinants derived from the spatial normalization in order to preserve the total amount of grey matter from the original images. Modulated images were smoothed with a Gaussian kernel (8 mm FWHM).

After discarding the first 8 volumes of each run, RSFC images were slice time corrected, spatially realigned, and skull-stripped. Subsequently, the mean functional image was coregistered with the T1-weighted, skull-stripped structural image, normalized and smoothed with a 6 mm full-width at half-maximum Gaussian kernel. The above pre-processing steps were performed in each participant's native space. Normalization was then completed by computing transformation parameters between the participant's T1

structural image and the MNI T1-weighted image template and applying the transformation to the functional resting-state scan. Next, CSF, white matter volumes, and the 6 motion parameters were estimated. The signal was band-pass filtered (0.008 Hz < f < 0.15 Hz) and nuisance variables, including the 6 motion parameters, CSF, and WM time-series, as well as the first derivative and quadratic terms, were regressed out from the data (Satterthwaite et al., 2013). The spectral filtering and nuisance regression was completed as a single step per suggestions by Hallquist, Hwang, & Luna, (2013).

Particular care was taken to check the quality of the RSFC scans to minimize the impact of head motion and scanning artifacts. All scans were visually inspected for artifacts, field inhomogeneity, incomplete skull stripping, and proper normalization. Scans with translational motion greater than 2 mm were discarded (n=11). For these participants, an additional database query was conducted to determine whether a second scan of adequate quality was available from a later time point in the longitudinal UCSF study. An acceptable alternate scan was available for a subset of participants (n=5). Subjects with translational motion between 1-2 mm, such that more than 10% of total time points for translational motion were greater than 1 mm, were also excluded (n=1), and a second time point included in the data set. No subjects had strong periodic movement; however, excessive rotational periodic movement (defined as ~0.5-1 mm rotation in a periodic fashion) was considered criterion for exclusion. Five subjects were excluded because of a revised PPA diagnosis since the collection of the original scan, and one subject was excluded because of poor image quality.

2.4.2. Step 2— Seed selection

We selected seeds for analysis within the dorsal and ventral language pathways that have converging evidence from structural analyses of atrophy in patients with language network dysfunction, as well as from functional neuroimaging of phonological-articulatory and lexical-semantic tasks in healthy participants (Figure 1). It is well documented that atrophy peaks are consistently observed in the left inferior frontal lobe, temporoparietal junction, and anterior temporal lobe in nfvPPA, lvPPA and svPPA patients, respectively (Gorno-Tempini et al., 2011). We chose seeds for ROIs in the IFG, area SPT and ATL that are also documented nodes of critical language networks for syntax, phonology and semantics and which overlapped with atrophy peaks in nfvPPA, lvPPA, and svPPA.

Figure 1: Regions of Interest for RSFC Analysis

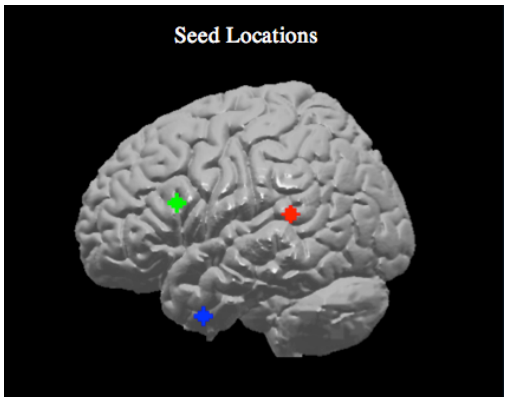

Spherical ROIs of 4 mm radius were located at MNI = (-40, 21, 20) for the IFG seed (shown in green), (-54, -39, 15) for area SPT seed (red) and (-51, 6, -39) for the ATL seed (blue).

2.4.2.1. Inferior frontal gyrus (IFG) seed

For nfvPPA, we chose coordinates from a cluster in the left dorsal posterior IFG (peak at MNI = -40, 21, 20) that was identified by Wilson et al., (2012) as a region modulated by syntactic complexity in healthy controls (but not nfvPPA) and also identified as atrophic in their nfvPPA patient group (Figure 1). Beyond that study, this area has converging evidence showing functional activation in healthy participants during syntactic processing and is also an area of peak atrophy in patients with nonfluent/agrammatic PPA (Gorno-Tempini et al., 2004; Liakakis, Nickel, & Seitz, 2011; Wilson et al., 2012).

2.4.2.2. Temporoparietal seed (area SPT)

For lvPPA, we chose a seed within the posterior Sylvian junction of the temporoparietal region (area SPT; Figure 1). This area is functionally implicated in core phonological tasks involving automated transfer of auditory representations into articulatory output; it is also a well-known area of peak atrophy in lvPPA (Buchsbaum & D'Esposito, 2008; Gorno-Tempini et al., 2011; Madhavan et al., 2013; Rohrer et al., 2013). Area SPT is implicated in auditory-motor integration for speech (as required for repetition) and is considered to be critically involved in phonological processing, a core deficit in lvPPA (Buchsbaum & D'Esposito, 2008; Gorno-Tempini et al., 2011; Henry & Gorno-Tempini, 2010; Hickok & Poeppel, 2007; Okada & Hickok, 2006; Peschke et al., 2012). We utilized an ROI for area SPT identified by Peschke et al., (2012) and defined by the average of MNI coordinates derived from nine previous studies, as area SPT is

functionally-derived and varies among individuals (Buchsbaum et al., 2005b, 2011; Buchsbaum, Olsen, Koch, & Berman, 2005a; Callan et al., 2006; Hickok, Buchsbaum, Humphries, Muftuler, 2003; Okada & Hickok, 2006; Okada, Smith, Humphries, & Hickok, 2003; Pa and Hickok, 2008; Wilson and Iacoboni, 2006). These averages yielded the coordinates MNI = -54, -39, 15, which we used as the center of a 4 mm spherical ROI.

2.4.2.3. Anterior temporal lobe (ATL) seed

For svPPA, we chose the coordinate MNI=-51, 6, -39 within the ATL as the center for a spherical 4 mm ROI (Figure 1). This was the peak of a cluster that was identified by Binney et al., (2010) from fMRI activation during semantic tasks in healthy controls; this area was also significantly atrophic in svPPA patients in the same study. Of particular note, a related study showed that repetitive transcranial magnetic stimulation (rTMS) to the same ATL coordinate in healthy participants resulted in deficits that mimicked svPPA semantic deficits. Converging evidence from voxel-based morphometry studies showing left lateralized atrophy in the ventral and lateral anterior temporal lobes for svPPA, functional imaging activation of the ATL during semantic tasks, and rTMS studies inducing semantic deficits via "virtual lesions" in the lateral left ATL support the role of the ATL in semantic processing and our choice of this seed for RSFC analysis (Campanella, Fabbro, & Urgesi, 2013; Galton et al., 2001; Gorno-Tempini et al., 2004; Hurley et al., 2015; Lambon Ralph, Pobric, & Jefferies, 2009; Mummery et al., 2000; Patterson et al., 2007; Pobric, Jefferies, & Ralph, 2007).

2.4.3. Step 3— Identify regions of atrophy in patient populations

Voxel-Based Morphometry (VBM): Following segmentation, we identified regions of reduced cortical volume using 2-sample *t*-tests in SPM, with age, sex, and total intracranial volume included as nuisance covariates. Analyses were corrected for multiple comparisons at the cluster level using family-wise error correction (FWE), $p<0.05$ and displayed with an extent threshold of 50 voxels.

2.4.4. Step 4— Delineate resting-state functional connectivity for seeds in each group

Spherical ROIs with 4-mm radius were created for IFG, SPT, and ATL coordinates and utilized in a whole-brain regression analysis for each participant. The average spontaneous BOLD signal time series from each ROI was correlated as a covariate of interest with each voxel's time series within the brain. Statistical analysis was conducted in SPM. A one sample *t*-test was conducted using the voxel-wise *z*-scores for each participant's resting-state functional connectivity map (per ROI) to derive group-level connectivity maps for each group. Results were inclusively masked by the MNI template brain. Age, sex, and total intracranial volume were included as covariates of no interest. Analyses were corrected for multiple comparisons at the cluster level using a threshold of $p<0.005$, with family-wise error (FWE) correction and extent threshold of 30 voxels. Group level connectivity maps for each seed were overlaid on maps derived from healthy controls and results visualized in XJView toolbox (http://www.alivelearn.net/xjview).

2.4.5. Step 5— Determine significant group differences in resting-state functional connectivity

To determine RSFC differences between each patient group and controls, we utilized the Biologic Parametric Mapping toolbox (BPM; http://www.nitrc.org/projects/rbpm) within SPM to estimate significant group differences while controlling for gray matter atrophy in patients (Casanova et al., 2007; Smieskova et al., 2012). This approach is particularly relevant in PPA, where different cortical regions in the brain can have vastly different amounts of degeneration, despite global similarity in gray matter volume. For our analysis, a one-way analysis of covariance (ANCOVA) was performed, with voxel-wise gray matter volume regressed out as a nuisance covariate, similar to methods used previously in FTD (Farb et al., 2013 and Premi et al., 2014). Age, sex, and total intracranial volume were included as non-imaging nuisance covariates in the ANCOVA model. Group level differences in functional connectivity networks between patient groups and controls were then calculated using a statistical threshold of $p<0.005$ (uncorrected) and extent threshold of 30 voxels. Consistent with other studies in frontotemporal dementia using a similar statistical approach, we utilized a relatively lenient statistical threshold of $p<0.005$ (uncorrected) in order to maximize visualization of between-group differences, while accounting for atrophy (Farb et al., 2013; Premi et al., 2014; Seeley et al., 2009). Whole brain *p*-values were extracted for Appendix tables using the BSPMView toolbox (http://www.bobspunt.com/bspmview/).

III. Results

3.1. Controls

The networks revealed by seed-based analyses in healthy controls were large and robust; as such, the results that follow represent a general overview of significant regions (see Figure 2).

Figure 2: IFG, SPT and ATL-seeded RSFC Networks for Healthy Controls

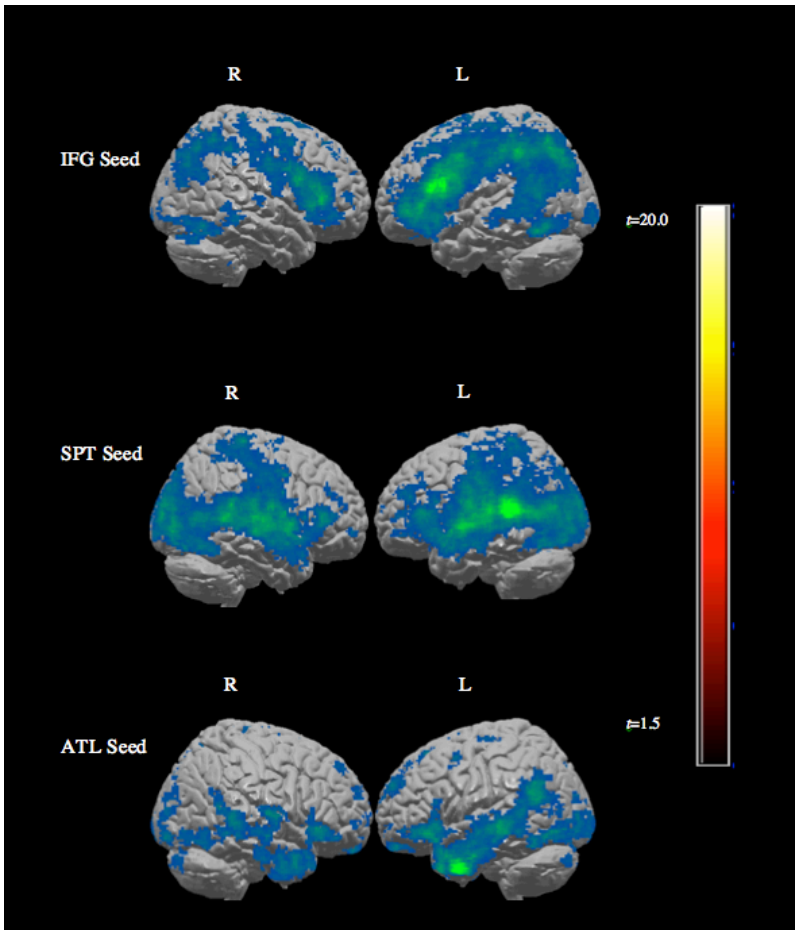

Analyses were corrected for multiple comparisons at the cluster level using family-wise error correction (FWE), $p<0.005$, with extent threshold of 30 voxels.

3.1.1. IFG-Seeded RSFC

The left IFG seed correlated with numerous regions within the left hemisphere, including and extending beyond the traditional perisylvian speech and language networks. Specifically, the seed in IFG was functionally connected with superior, middle, and inferior frontal gyri (i.e. SFG, MFG, & IFG), supplementary motor area (SMA), pre- and postcentral gyri, superior/inferior parietal lobe, posterior temporal lobe, and occipital regions. These regions are known to play a role in speech and language functions, and dorsal anatomical structures within these regions are often damaged in nfvPPA (Friederici & Gierhan, 2013; Gorno-Tempini, 2011). A similar but less robust network was observed in the right hemisphere, encompassing MFG, IFG, pre- and postcentral gyri, superior parietal, inferior temporal, and occipital regions. Subcortically, significant correlations were observed bilaterally in the left and right caudate and putamen (Appendix Table A2).

3.1.2. SPT-Seeded RSFC

This seed also correlated with a large, bilateral network including left perisylvian speech-language regions and homologous right regions. Specifically, significant connectivity was seen bilaterally along the MFG, IFG, STG, MTG, pre- and postcentral gyri, temporoparietal cortex, and occipital lobe, as well as the left hippocampus and amygdala. Subcortically, the thalamus and putamen showed significant correlations bilaterally. The seed in area SPT correlated with frontal regions regions integral to motor speech and posterior regions involved in auditory processing, consistent with the role of

area SPT as a sensory-motor interface for speech processing (Hickok et al., 2009; Puce et al., 1995; Appendix Table A3).

3.1.3. ATL-Seeded RSFC

The left ATL seed showed a functional connectivity pattern that differed greatly from those observed for IFG/SPT and included several areas integral for semantic cognition (Binder et al., 2009). The ATL seed correlated with left temporal, temporoparietal, and inferior temporo-occipital cortices, as well as the IFG/orbitofrontal cortex. Significant right hemisphere correlations were observed in homologous frontal, temporal, and occipital regions (Appendix Table A4).

3.2. NON-FLUENT VARIANT PPA

3.2.1. VBM Results

Consistent with our hypothesis, VBM revealed significant atrophy in nfvPPA relative to controls in the left insula, IFG, pre- and postcentral gyri, SMA, and basal ganglia (Gorno-Tempini et al., 2004). Right hemisphere areas of significant atrophy were less robust and included the MFG, SFG, insula, precentral gyrus, and basal ganglia (Figure 3; Appendix Table A5).

Figure 3: VBM of Brain Atrophy within Three Variants of PPA, as Compared to Controls

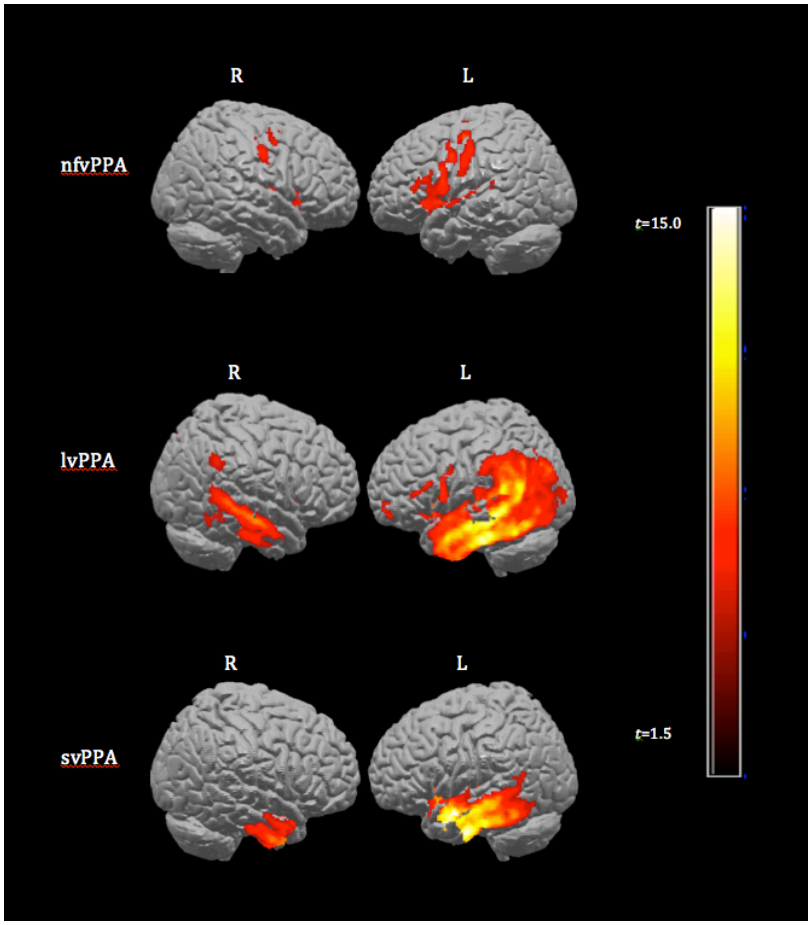

Analyses were corrected for multiple comparisons at the cluster level using family-wise error correction (FWE), $p<0.005$, with extent threshold of 50 voxels.

3.2.2. Seed Analyses— IFG Seed

The IFG-seeded network in nfvPPA significantly overlapped with the healthy control map, with less extensive correlation with posterior temporal and parietal regions bilaterally. Robust frontal lobe correlations with the IFG seed extended beyond the control network into the anterior SFG, suggesting active recruitment of the frontal lobes to compensate for reduced temporoparietal connectivity (Appendix Table A6).

Direct comparison of IFG-seeded networks between nfvPPA and healthy controls, while controlling for gray matter volume, revealed significant reductions in connectivity in right orbitofrontal cortex and precuneous (Figure 4; Appendix Table A7).

Figure 4: IFG-seeded RSFC Networks for nfvPPA and Corresponding Group Differences

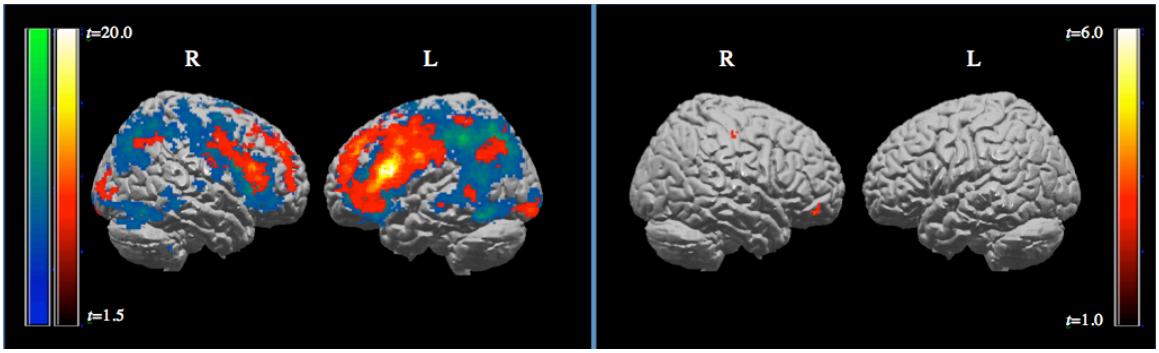

(Left) IFG-seeded RSFC networks for nfvPPA (in red-yellow) overlaid on homologous networks derived from healthy controls (in blue-green). Analyses were corrected for multiple comparisons at the cluster level using family-wise error correction (FWE), $p<0.005$, with extent threshold of 30 voxels. (Right) Statistically significant group level differences in IFG-seeded RSFC networks for nfvPPA and controls, with gray matter as an imaging covariate. Analyses were calculated using a statistical threshold of $p<0.005$ (uncorrected), with an extent threshold of 30 voxels.

3.2.3. Seed Analyses— SPT seed

RSFC networks from the temporoparietal seed in nfvPPA showed significant overlap with healthy control networks in perisylvian regions bilaterally, with less extension dorsally and anteriorly into extrasylvian regions (Appendix Table A8).

A group level statistical comparison between nfvPPA and healthy controls for IFG-seeded networks revealed significant reductions in connectivity within bilateral cingulate gyrus and caudate, as well as right pre- and postcentral gyri, after correcting for the effects of atrophy (Figure 5; Appendix Table A9).

Figure 5: SPT-seeded RSFC Networks for nfvPPA and Corresponding Group Differences

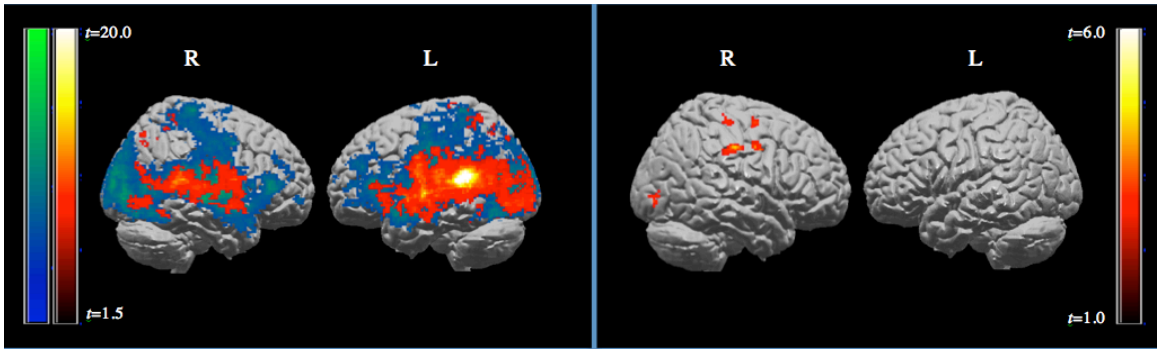

(Left) SPT-seeded RSFC networks for nfvPPA (in red-yellow) overlaid on homologous networks derived from healthy controls (in blue-green). Analyses were corrected for multiple comparisons at the cluster level using family-wise error correction (FWE), $p<0.005$, with extent threshold of 30 voxels. (Right) Statistically significant group level differences in SPT-seeded RSFC networks for nfvPPA and controls, with gray matter as an imaging covariate. Analyses were calculated using a statistical threshold of $p<0.005$ (uncorrected), with an extant threshold of 30 voxels.

3.2.4. Seed Analyses— ATL-Seed

The ATL-seeded network in nfvPPA showed significant overlap with the healthy control map in bilateral temporal regions, as well as left IFG/orbitofrontal cortex and temporoparietal junction (Appendix Table A10).

A statistical comparison of ATL-seeded RSFC networks in healthy controls and nfvPPA after correcting for atrophy revealed significant reductions in connectivity in the right postcentral gyrus. Alterations in connectivity were also seen in the left caudate nucleus and bilateral cingulate (Figure 6; Appendix Table A11).

Figure 6: ATL-seeded RSFC Networks for nfvPPA and Corresponding Group Differences

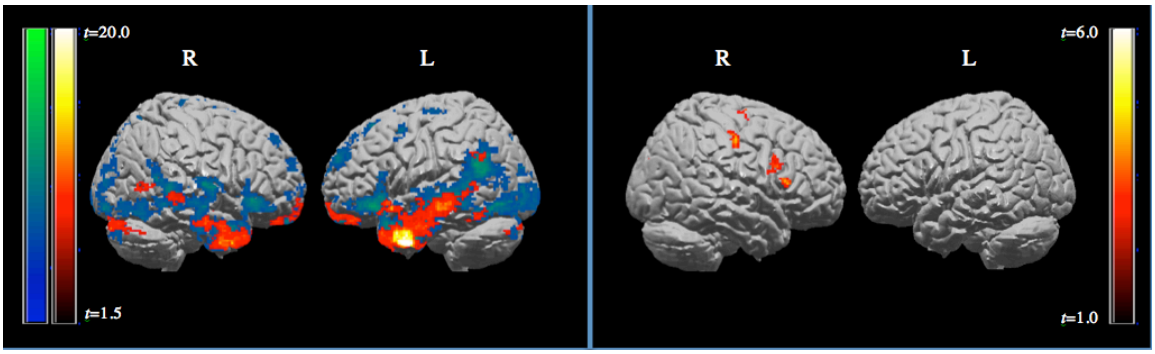

Left) ATL-seeded RSFC networks for nfvPPA (in red-yellow) overlaid on homologous networks derived from healthy controls (in blue-green). Analyses were corrected for multiple comparisons at the cluster level using family-wise error correction (FWE), $p<0.005$, with extent threshold of 30 voxels. (Right) Statistically significant group level differences in ATL-seeded RSFC networks for nfvPPA and controls, with gray matter as an imaging covariate. Analyses were calculated using a statistical threshold of $p<0.005$ (uncorrected), with an extant threshold of 30 voxels.

3.3. Logopenic Variant PPA

3.3.1. VBM results

Consistent with previous literature, the lvPPA patient group demonstrated significant atrophy throughout left temporal and temporoparietal cortex (see Figure 3; Rohrer et al., 2013; Rogalski et al., 2011, 2014). Additional regions of atrophy included smaller clusters in the left frontal operculum, IFG and bilateral insula. Less extensive right hemisphere atrophy was observed in the MTG, ITG, inferior parietal lobe, precuneus, and cingulate. Subcortically, lvPPA had significant gray matter loss in the left caudate and bilateral thalamus (Appendix Table A12).

3.3.2. Seed Analyses— IFG-Seed

In lvPPA, the IFG-seeded network was substantially reduced compared to the network revealed by controls and encompassed small areas within the frontal lobes, including left hemisphere IFG, MFG, and frontal operculum, as well as right IFG and MFG (Appendix Table A13).

Between-group differences for IFG-seeded networks in lvPPA and healthy controls revealed reduced functional connectivity primarily in the bilateral superior parietal cortices, precuneus and temporal poles, after correcting for the effects of atrophy. Reduced connectivity was also observed in left temporoparietal and orbitofrontal regions, as well as bilateral occipital and cerebellar regions (Figure 7; Appendix Table A14).

Figure 7: IFG-seeded RSFC Networks for lvPPA and Corresponding Group Differences

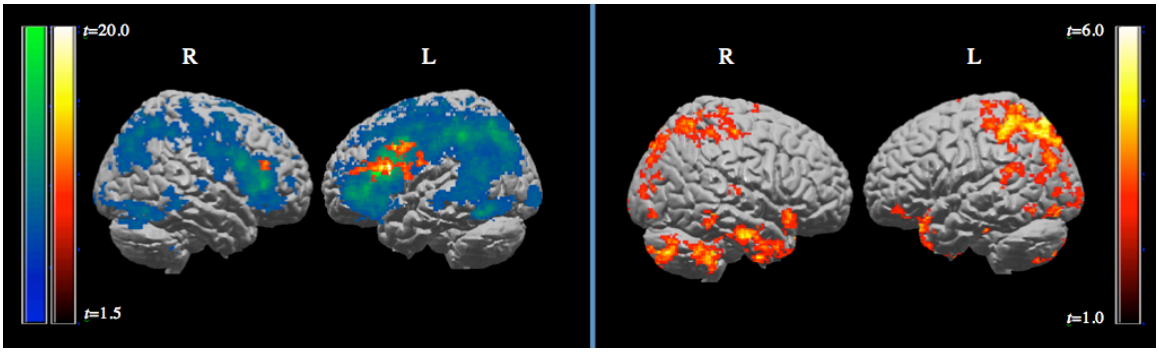

(Left) IFG-seeded RSFC networks for lvPPA (in red-yellow) overlaid on homologous networks derived from healthy controls (in blue-green). Analyses were corrected for multiple comparisons at the cluster level using family-wise error correction (FWE), $p<0.005$, with extent threshold of 30 voxels. (Right) Statistically significant group level differences in IFG-seeded RSFC networks for lvPPA and controls, with gray matter as an imaging covariate. Analyses were calculated using a statistical threshold of $p<0.005$ (uncorrected), with an extant threshold of 30 voxels.

3.3.3. Seed Analyses— SPT-Seed

Similar to results in the IFG-seeded network, significant correlations to the SPT seed were highly reduced and consisted of a left lateralized focal cluster at the temporoparietal junction, with extension into the postcentral gyrus (Appendix Table A15).

A group-level statistical comparison of SPT-seeded networks in healthy controls and lvPPA with atrophy correction revealed bilateral but right-dominant reductions in connectivity clustered around the right motor strip, SMA, and STG. Small clusters were seen dorsally in the frontal (bilateral SFG, MFG, IFG), temporal (bilateral STG and right ITG), and bilateral superior parietal, and occipital lobes, with additional statistically significant network alterations in right precuneous and caudate and left cingulate (Figure 8; Appendix Table A16).

Figure 8: SPT-seeded RSFC Networks for lvPPA and Corresponding Group Differences

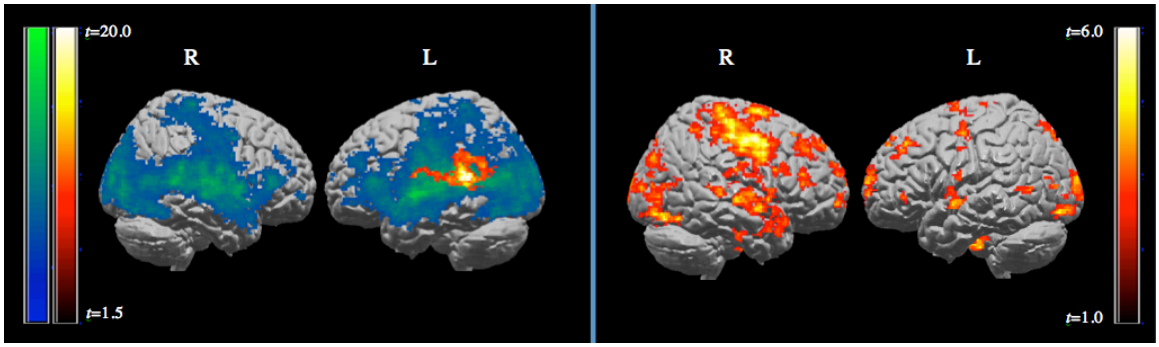

(Left) SPT-seeded RSFC networks for lvPPA (in red-yellow) overlaid on homologous networks derived from healthy controls (in blue-green). Analyses were corrected for multiple comparisons at the cluster level using family-wise error correction (FWE), $p<0.005$, with extent threshold of 30 voxels. (Right) Statistically significant group level differences in SPT-seeded RSFC networks for lvPPA and controls, with gray matter as an imaging covariate. Analyses were calculated using a statistical threshold of $p<0.005$ (uncorrected), with an extant threshold of 30 voxels.

3.3.4. Seed Analyses— ATL-Seed

Connectivity relative to the ATL seed was substantially reduced and very focal. Significant correlations were seen within and immediately adjacent to the seeded region in the ATL (Appendix Table A17).

A group-level statistical comparison between lvPPA and healthy controls for ATL-seeded networks revealed large alterations in connectivity primarily within the right STG, bilateral MTG, and left occipital lobe, after correcting for atrophy. Additional group differences were seen bilaterally in the SMA, as well as in the left IFG/frontal operculum and postcentral gyrus. Dorsal right hemisphere reductions in connectivity were noted in the superior parietal lobes and insula (Figure 9; Appendix Table A18).

Figure 9: ATL-seeded RSFC Networks for lvPPA and Corresponding Group Differences

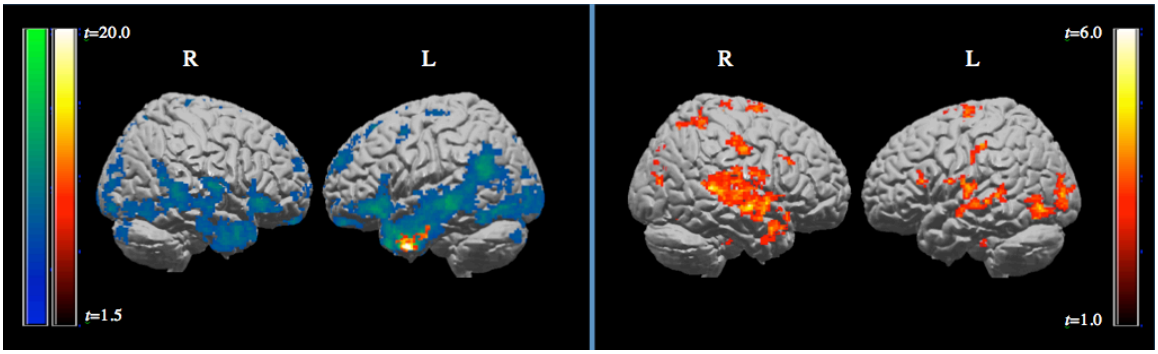

(Left) ATL-seeded RSFC networks for lvPPA (in red-yellow) overlaid on homologous networks derived from healthy controls (in blue-green). Analyses were corrected for multiple comparisons at the cluster level using family-wise error correction (FWE), $p<0.005$, with extent threshold of 30 voxels. (Right) Statistically significant group level differences in ATL-seeded RSFC networks for lvPPA and controls, with gray matter as an imaging covariate. Analyses were calculated using a statistical threshold of $p<0.005$ (uncorrected), with an extant threshold of 30 voxels.

3.4. Semantic Variant PPA

3.4.1. VBM Results

Consistent with our hypothesis, areas of significant atrophy relative to healthy controls included a large cluster involving the left ventrolateral temporal lobe, hippocampus/amygdala, and insula, as well as a smaller right anterior and ventral temporal lobe cluster. Subcortical atrophy was also observed in the left caudate and putamen (Figure 3; Appendix Table A19).

3.4.2. Seed Analyses— IFG Seed

The IFG-seeded network in svPPA overlapped with the control network primarily in frontal dorsal areas within the left MFG/IFG. Correlations with the ATL seed were

seen to a lesser extent in the left superior parietal lobe and smaller clusters were observed in the right hemisphere MFG/IFG, as well as bilateral SMA and calcarine fissure (Appendix Table A20).

A group level statistical comparison between svPPA and healthy controls for IFG-seeded networks revealed significant reductions in connectivity within the left anterior inferior temporal pole and cerebellum (Figure 10; Appendix Table A21).

Figure 10: IFG-seeded RSFC Networks for svPPA and Corresponding Group Differences

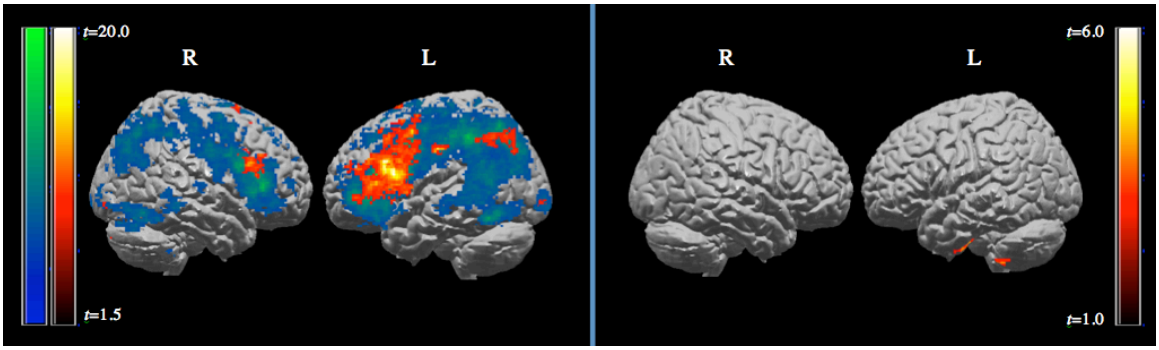

(Left) IFG-seeded RSFC networks for svPPA (in red-yellow) overlaid on homologous networks derived from healthy controls (in blue-green). Analyses were corrected for multiple comparisons at the cluster level using family-wise error correction (FWE), $p<0.005$, with extent threshold of 30 voxels. (Right) Statistically significant group level differences in IFG-seeded RSFC networks for svPPA and controls, with gray matter as an imaging covariate. Analyses were calculated using a statistical threshold of $p<0.005$ (uncorrected), with an extant threshold of 30 voxels.

3.4.3. Seed Analyses— SPT Seed

The SPT-seeded network in svPPA overlapped with, but was less extensive than the SPT-seeded network in healthy controls. Networks within svPPA extended bilaterally across perisylvian regions from the temporoparietal junction into posterior temporal, inferior frontal, and parietal areas. SPT-seeded networks in extrasylvian areas included a

small cluster within the right dorsal motor strip, well as larger bilateral clusters in the occipital lobe (Appendix Table A22).

Between-group statistical analyses for SPT-seeded networks in svPPA versus healthy controls with atrophy correction revealed reductions in connectivity for small clusters within the left anterior MTG, ITG and right pre- and postcentral gyri as well as bilateral cerebellum (Figure 11; Appendix Table A23).

Figure 11: SPT-seeded RSFC Networks for svPPA and Corresponding Group Differences

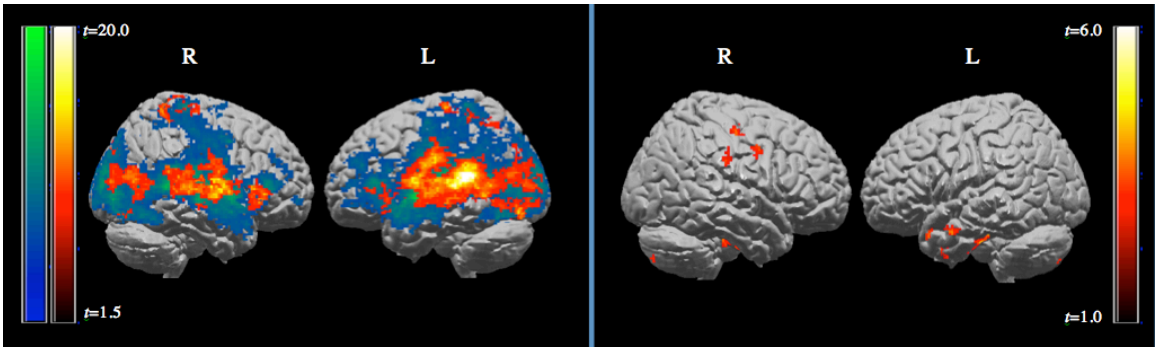

(Left) SPT-seeded RSFC networks for svPPA (in red-yellow) overlaid on homologous networks derived from healthy controls (in blue-green). Analyses were corrected for multiple comparisons at the cluster level using family-wise error correction (FWE), $p<0.005$, with extent threshold of 30 voxels. (Right) Statistically significant group level differences in SPT-seeded RSFC networks for svPPA and controls, with gray matter as an imaging covariate. Analyses were calculated using a statistical threshold of $p<0.005$ (uncorrected), with an extant threshold of 30 voxels.

3.4.4. Seed Analyses— ATL Seed

Functional connectivity within the ATL-seeded network in svPPA was substantially reduced relative to healthy controls and presented with focal connectivity in the temporal pole within regions immediately surrounding the seed (Appendix Table A24).

A direct comparison using BPM revealed significant group differences in connectivity within left perisylvian regions (IFG, pre-/postcentral gyri, STG, and temporoparietal junction) as well as the posterior inferior temporal cortex. A subset of homologous frontal, parietal, and temporal regions had significantly reduced connectivity in the right hemisphere (Figure 12; Appendix Table A25).

Figure 12:ATL-seeded RSFC Networks for svPPA and Corresponding Group Differences

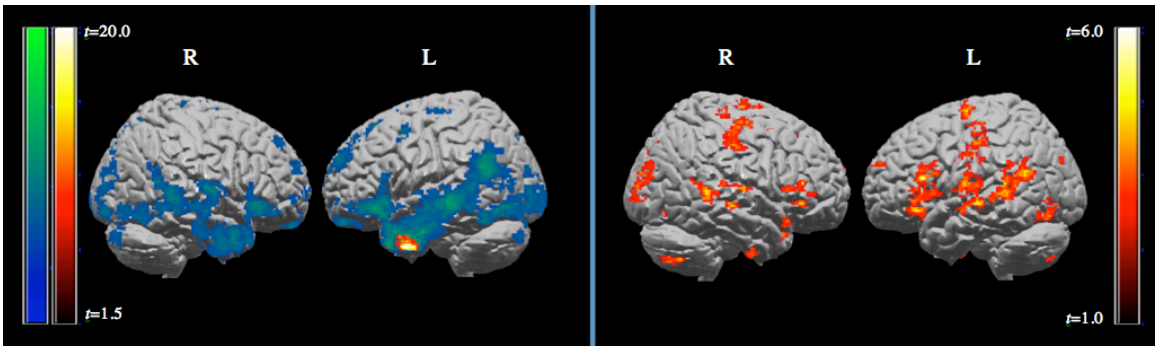

(Left) ATL-seeded RSFC networks for svPPA (in red-yellow) overlaid on homologous networks derived from healthy controls (in blue-green). Analyses were corrected for multiple comparisons at the cluster level using family-wise error correction (FWE), $p<0.005$, with extent threshold of 30 voxels. (Right) Statistically significant group level differences in ATL-seeded RSFC networks for svPPA and controls, with gray matter as an imaging covariate. Analyses were calculated using a statistical threshold of $p<0.005$ (uncorrected), with an extant threshold of 30 voxels.

IV. Discussion

Imaging studies in PPA have shown that PPA targets specific sub-networks within the general language network through targeted neurodegeneration (Seeley et al., 2009). Despite well-documented patterns of structural decline in PPA, no studies have examined patterns of functional connectivity or their alteration in each of the clinical variants. In this study, we investigated resting-state functional connectivity (RSFC) networks via seeds representing key nodes of the dorsal and ventral language streams within PPA variants and healthy controls. We analyzed group-level gray matter loss and included gray matter volume as an imaging covariate to measure network-wide RSFC disruptions in PPA above and beyond the effects of atrophy for three language seeds (IFG, SPT, and ATL).

On the basis of well-established behavioral profiles and patterns of atrophy within variants (Gorno-Tempini et al., 2004, 2011), we hypothesized that nfvPPA would exhibit atrophy primarily in the dorsal articulatory-phonological language pathway. We predicted that lvPPA would have similar atrophy in the dorsal articulatory-phonological pathway, with some extension into the ventral pathway. Although historically, lvPPA was associated with predominant left posterior perisylvian/temporoparietal atrophy, (Gorno-Tempini et al., 2008; 2011), more recent papers document involvement of both temporoparietal regions and the temporal lobe, particularly with disease progression (Rohrer et al., 2013; Rogalski et al., 2011). Lastly, we predicted that atrophy within svPPA would be confined to the ventral lexical-semantic pathway. We hypothesized that

RSFC networks derived from language network seeds would be less extensive in patients relative to controls and, with regard to specific patterns of RSFC alteration in each variant, we hypothesized that: (1) nfvPPA group would have widespread disruption in functional connectivity primarily within dorsally seeded articulatory-phonological networks (IFG and SPT seeds), (2) lvPPA would show prominent disruption in the network derived from dorsal (SPT and IFG) seeds, with lesser alteration of the ventrally seeded (ATL) network and, (3) svPPA would have widespread disruptions primarily in the ventrally seeded semantic network (ATL seed).

4.1. Extent of Atrophy in PPA Variants

Findings from our voxel-based morphometry (VBM) analyses were consistent with well-established atrophy patterns in each of the PPA variants. The nfvPPA group displayed significant atrophy in a circumscribed region within the dorsal articulatory-phonological pathway (left IFG, motor strip, basal ganglia and, to a lesser extent, STG). The lvPPA group demonstrated atrophy affecting bilateral temporal and parietal regions and, to a lesser extent left IFG, implicating both dorsal and ventral language pathways[3]. Finally, the svPPA group displayed significant atrophy in bilateral anterior temporal regions within the ventral lexical-semantic pathway.

[3] The patient scans included in the current study were acquired at the earliest available time point relative to the patient's first visit in a longitudinal study at UCSF. It is worth noting that lvPPA shares pathology with early-onset AD and presents with similar behavioral features, including early word finding deficits. In fact, many lvPPA patients are misdiagnosed as typical AD and thus do not receive a correct diagnosis until language symptoms have progressed to a greater degree. It is possible that our lvPPA cohort was referred to UCSF at a later date post-onset than nfvPPA or svPPA, and thus presented with more extensive atrophy. This is supported by the finding of worse *MMSE* scores in the lvPPA group relative to the other patient cohorts (Table 1).

4.2. RSFC NETWORKS IN HEALTHY SUBJECTS

RSFC networks derived from dorsal (IFG and SPT) seeds in healthy controls included areas associated with articulatory-phonological and motor speech pathways, but were extensive and encompassed other areas within and beyond the traditional language network. Networks derived from SPT and IFG overlapped substantially in the left hemisphere, suggesting a highly interconnected and bidirectional phonological-articulatory network. Areas found in SPT and IFG-seeded networks included the bilateral MFG/IFG, pre- and post-central gyri, superior/inferior parietal lobe, posterior temporal lobe, and occipital lobe. Additional regions that correlated with the IFG seed included bilateral SMA, superior frontal gyrus, and caudate and putamen. The SMA is crucial in the "programming" and fluent use of intentional speech (Goldberg, 1985). In contrast, the putamen is thought to control cortical initiation (Booth, Wood, Lu, Houk & Bitan, 2007), with activation of the left basal ganglia observed in syntactic relative to semantic tasks (Friederici, Ruschemeyer, Hahne & Fiebach, 2003). Unlike the IFG-seeded network, the SPT-seeded network included bilateral mid-to-anterior STG/MTG. The STG has been implicated in a variety of language functions, with the posterior part of the superior temporal gyrus selectively activated by sentence and text processing, while the superior and middle temporal sulcus are activated in phonological tasks (Vigneau et al., 2006).

The SPT-seeded network also included the hippocampus, amygdala and thalamus, regions not commonly seen in the traditional language network. An important methodological limitation is that our statistical threshold (p<0.005 FWE) was selected with the goal of sensitivity in both patient and control groups (to allow for direct

comparison in healthy versus disease groups). This threshold was, in effect, overly lenient for controls, producing results that obscured patterns within specific dorsal sub-networks. Future research should explore RSFC maps derived from seeds in healthy controls at a more stringent threshold to allow for more fine-grained analysis of shared versus unique anatomical regions in these two seeded networks specifically.

Relative to existing RSFC studies in healthy controls, our IFG and SPT-seeded networks overlapped with, but were more extensive than other studies investigating seed-based functional connectivity in healthy controls. In a landmark study, Tomasi & Volkow (2012) compared resting-state networks using traditional language seeds, e.g. Broca's area and Wernicke's area, in 970 healthy subjects from over 22 research centers across the world. The seed they used Broca's area was within the IFG and similar to our IFG seed, with spherical radius ~4mm (ROI volume=3.375 cm^3). The other seed, referred to as Wernicke's area, was slightly superior to our SPT seed, located in the supramarginal gyrus. Tomasi & Volkow found connectivity within adjoining prefrontal, temporal and parietal regions, similar to the current study results, as well as additional bilateral caudate, left putamen and subthalamic nuclei connectivity, for both Broca's and Wernicke's area seeds. Tomasi & Volkow's networks did not have positive correlations in the post-central gyrus, SMA, or occipital lobe for Broca's seeded-networks. Similarly, no positive correlations were noted in the Wernicke's-seeded network in the post-central gyrus, superior temporal lobe, or occipital lobe. Research has shown that the IFG has a highly specialized, differential function within the pars triangularis, opercularis, and orbitalis (Vigneau et al., 2006). This is important in the context of seed analysis for

RSFC, as slightly different coordinates can drastically change resulting networks. Some variability is expected between studies.

RSFC for the ATL-seeded network in healthy controls included a network of regions implicated in semantic processing, as well as additional regions involved in comprehension and production of spoken and written language more broadly: bilateral temporal, dorsal and inferior frontal, inferior parietal, and temporo-occipital regions. Our ATL-seeded RSFC network corresponded to other RSFC networks produced in healthy controls within the literature. Jackson, Hoffman, Pobric, & Lambon Ralph (2016) analyzed and compared ATL-seeded RSFC networks in 78 healthy subjects with functional imaging of the same cohort while they performed semantic tasks using a variety of modality-specific stimuli including pictorial, linguistic auditory and environmental auditory stimuli. RSFC using a left ventral ATL-seed corresponded to regions active during functional neuroimaging of semantic tasks, including bilateral ATL, IFG, AG, posterior MTG, and medial temporal lobe connectivity, with additional frontal and occipital activation during task states. Our ATL-seeded network demonstrated substantial congruence to the Jackson et al. network but extended more broadly to additional occipital regions with no medial prefrontal connectivity. Once again, slight variation in seed locations can produce different networks. Additional RSFC studies with healthy controls, such as Hurley et al. (2015) found bilateral but asymmetrical connectivity between the left and right ATL, IFG, MTG, AG, and superior frontal gyrus. Reciprocal asymmetric left hemisphere involvement of the ATL within separate IFG and MTG-seeded networks showed that the ATL was directly connected to the language

network and should be considered an integral node within the classically defined language system. Here again, our ATL-seeded network supports this claim, with bilateral but asymmetric connectivity between the left ATL and perisylvian language network, as well as with the posterior inferior temporal lobe and occipital lobe.

Large portions of the temporal lobe have been implicated in a wide variety of semantic processing tasks. Sensory-motor representations from multiple areas of the brain are bound together in the ATL for subsequent use more broadly during semantic tasks or language processing (Lambon Ralph, Sage, Jones, & Mayberry, 2010; Rogers et al., 2004). Overall patterns of connectivity from the ATL to other modality-specific regions support the concept of the ATL as a "hub" for creating multimodal semantic representations (Hurley et al., 2015; Patterson et al., 2007; Jackson et al., 2016; Visser & Lambon Ralph, 2011).

Non-temporal areas connected within the ATL-seeded network are also implicated in the semantic network, but within the context of executive semantic retrieval and control. The angular gyrus (AG), which is situated between adjoining spatial, auditory, somatosensory and visual association areas, is purported to play a role in conceptual integration (Binder et al., 2009). Together with the prefrontal cortex and posterior MTG, the dorsal AG acts to "regulate and shape activation within the semantic system" (Noonan, Jefferies, Corbett & Lambon Ralph, 2010). Multiple functional imaging studies have implicated the IFG, specifically the "pars orbitalis," in semantic processing, particularly in the context of speech production tasks (Liakakis et al., 2011). However, the IFG and AG do not act as storage for semantic representations. IFG lesions

typically impair phonological, articulatory or syntactic processes, not core semantic knowledge (Binder, Desai, Graves & Contant, 2009). Instead, the IFG and AG act in conjunction with the ATL to retrieve, control, and manipulate lexical-semantic representations.

4.3. Relationship Between Atrophy and Resting-State Functional Connectivity in PPA

Consistent with our hypothesis, RSFC networks for all seeds were substantially less extensive in patients than controls. Visual inspection revealed that patients with the least extensive atrophy, i.e. nfvPPA, had the most robust networks compared to other variants. In contrast, lvPPA, the group with the most atrophy, had very reduced, focal networks compared to controls. Group-level statistical comparisons between controls and patients using BPM (to include gray matter volumes as a covariate) support this claim. The nfvPPA group had virtually no statistically significant differences compared to controls after controlling for atrophy, whereas lvPPA had significant and diffuse differences in connectivity throughout both hemispheres for all seeded-networks. For all variants, seeds overlapping with regions of atrophy were the most significantly altered as compared to controls, even after regressing out the effects of atrophy. This is consistent with Seeley's network degeneration hypothesis, whereby progressive atrophy targets specific networks, thereby causing network-wide disruption (Seeley et al., 2009).

Although patients displayed extensively limited network connectivity, group differences between patients and controls did not support selective ventral and dorsal

deficits by variant, contrary to our hypothesis. Our findings suggest that both ventral and dorsal language pathways are affected by left hemisphere atrophy, irrespective of clinical variant. In fact, seeded networks not within a direct region of atrophy were substantially reduced relative to controls, regardless of whether the variant demonstrated phonological-articulatory vs. lexical-semantic deficits. Together, these findings indicate that RSFC within dorsal and ventral language pathways are highly interconnected. Further, atrophy and RSFC both have unique neuroimaging signatures with an emerging logical relationship to one another and to clinical phenotype.

4.3.1. Non-Fluent Variant PPA

The nfvPPA group displayed the most robust networks of all patient groups, likely as a result of relatively less atrophy. Atrophy peaks were primarily in the insula, IFG, MFG, motor strip, SMA, and basal ganglia, which is consistent with the presence of both linguistic (syntactic) and motoric (AOS and dysarthria) deficits in this population (Gorno-Tempini, et al., 2004; Josephs, et al., 2006).

Resting-state networks in nfvPPA that were seeded in relatively spared, non-atrophic regions, i.e. SPT and ATL, were visually similar but still less extensive than control networks. RSFC networks for SPT encompassed perisylvian regions, with less extensive connectivity to extrasylvian regions such as the superior motor strip and dorsal frontal and parietal lobes, whereas RSFC networks for ATL extended into the bilateral temporal lobe, left IFG, orbitofrontal cortex and temporoparietal regions. Interestingly, positive correlations with dorsal regions in the frontal and parietal lobes were for the

most part markedly absent in both SPT and ATL seeded networks. This included absent connectivity in the left and right superior motor strip for SPT seeded networks, consistent with motor speech deficits (Gorno-Tempini et al., 2011). Additional, secondary bilateral anterior superior frontal recruitment was also noted for the IFG-seeded network. The superior frontal gyrus is thought to contribute to higher cognitive functions and working memory (Du Boisgueheneuc et al., 2006). Classic descriptions of the phonological loop implicate posterior temporoparietal regions in short-term phonological memory and frontal cortices with subvocal phonological rehearsal that serves to refresh the phonological memory store (Baddeley, 2003). Dorsal frontal recruitment may reflect compensatory working memory to support phonological working memory in the face of reduced fronto-parietal connectivity. This is consistent with results from Premi et al., (2014), which showed increased frontal recruitment for asymptomatic carriers of GRN+ mutated gene in FTD patients (including nfvPPA) relative to healthy controls.

Very small significant left hemisphere differences were seen in the basal ganglia (SPT seed: bilateral cingulate gyrus and caudate; ATL seed: left caudate nucleus). Recent research has implicated the basal ganglia in motor "chunking," which is important for the execution of articulatory targets with varying syntax (Wymbs, Bassett, Mucha, Porter, & Grafton, 2012). Motor "chunking" involves parsing knowledge of motor sequences into smaller morphemes, as needed for syntactic functions, by the left fronto-parietal network (Clerget, Poncin, Fadiga, & Olivier, 2012; Sakai, Kitaguchi, & Hikosaka, 2003; Verwey, 2001; Verwey & Eikelboom, 2003). The fronto-parietal network sends these short chunks to the basal ganglia to concatenate into longer clusters for use (Sakai et al. 2003; Verwey

1996). Although most frequently investigated in Parkinson's disease patients, breakdown in the ability to concatenate syntactic morphemes in the basal ganglia could result in agrammatic speech, as commonly seen in nfvPPA patients (Zenon & Olivier, 2014). Further research is needed to identify the RSFC interrelationship between basal ganglia and areas associated with articulation and phonology.

4.3.2. Logopenic Variant PPA

The lvPPA group demonstrated the most extensive atrophy, encompassing most of the left temporal lobe and extending dorsally into temporoparietal and frontal regions. Atrophy within both ventral and dorsal language streams appeared to reduce connectivity throughout left hemisphere areas associated with phonology (IFG seed: posterior STG; SPT seed: mid-STG, IFG; ATL seed: operculum) and semantics (IFG seed: ATL; ATL seed: MTG) (Vigneau et al., 2006). Although semantic processing is not usually impaired in lvPPA, phonological processing is a hallmark symptom in this patient group (Henry et al., 2016). As previously mentioned, classic "phonological loop" literature postulates that posterior temporoparietal regions serve as the center of short-term phonological storage, and frontal cortices mediate subvocal phonological rehearsal that serves to refresh the store (Baddeley, 2003). Alterations in connectivity between IFG, SPT, and the posterior superior temporal gyrus is consistent with prominent language deficits in lvPPA observed on phonological processing tasks such as repetition and visual and auditory word span tasks (Bookheimer, Zeffiro, Blaxton, Gaillard, Theodore, 2000; Buchsbaum, Hickok, & Humphries, 2001; Gorno-Tempini et al., 2011). With impaired short-term phonological

storage, individuals with lvPPA may be unable to refresh the store as easily, leading to repetition and comprehension deficits, particularly for longer sentences (Rohrer et al., 2010; Gorno-Tempini et al., 2008). Nonword reading is also impaired in lvPPA, due to the increased phonological demands when decoding nonwords (Henry et al., 2016). The operculum is heavily implicated in phonological processing and nonword reading (Chein, Fissell, Jacobs, & Fiez, 2002; Fiez, Tranel, Seager-Frerichs, & Damasio, 2006; Jobard, Crivello, & Tzourio-Mazoyer, 2003; Vigneau, et al., 2006). As such, differences in connectivity with the operculum is consistent with selective nonword reading deficits. Our cohort also demonstrated significantly reduced connectivity between the ATL and MTG, areas that are key for semantic processing (Binder, Desai, Graves, & Conant, 2009). LvPPA patients do not usually display semantic deficits (Gorno-Tempini, 2011) early in the disease course, but may develop comprehension deficits later in the progression. As such, reduced connectivity in the ventral pathway may reflect a more advanced disease state in this specific patient group. This is supported by the finding of lower *MMSE* scores in lvPPA relative to healthy controls, nfvPPA and svPPA groups.

4.3.3. Semantic Variant PPA

Consistent with results from the other three variants, resting-state networks for all three seeds were substantially less extensive in svPPA, despite only ventral damage within the ATL. As would be expected, the ATL-seeded network was the most substantially reduced. However, dorsal seeded networks, (i.e IFG and SPT) were also substantially limited compared to controls upon visual inspection. Dorsally seeded

networks had few statistically significant group-level differences after controlling for the effects of atrophy. In the ATL-seeded network, altered connectivity was widely distributed throughout the language network, as compared to controls, and included the left hemisphere IFG, posterior ITG, pre-motor areas, and STG. Network-wide dysfunction was not limited to the ventral stream only. Reductions in connectivity between the ATL and posterior inferior temporal cortex, a region in the ventral stream believed to be a semantic-lexical interface (Hickok, 2012), is consistent with comprehension deficits in svPPA (Gorno-Tempini et al., 2011). Disruption in connectivity between the ATL and IFG within the ATL-seeded network may be indicative of impaired lexical retrieval and semantic control, as IFG and MTG are thought to control lexical-semantic access (Noonan, Jefferies, Visser, & Lambon Ralph, 2013; Wagner, Paré-Blagoev, Clark, & Poldrack, 2001). This hypothesis is bolstered by fMRI results in healthy controls on semantic tasks such as delayed copy drawing and object recognition, which require manipulation and use of salient semantic features (Patterson et al., 2007). Within this model, the ATL "hub" interacts with modality-specific regions to create coherent semantic concepts, whereas the frontal and parietal cortices control facilitated retrieval and use of such concepts (Jefferies, 2013; Lambon Ralph, 2014; Noonan et al., 2010; Noonan et al., 2013; Patterson, Nestor, & Rogers, 2007; Thompson-Schill, D'Esposito, & Kan, 1999; Wagner et al., 2001). The IFG-seeded RSFC network showed significant differences in connectivity with the ATL in svPPA compared to controls. Interestingly, the SPT-seeded RSFC network also showed altered connectivity with the ATL, indicating that the ATL and IFG/SPT, respectively, are

interconnected within a bidirectional language network, consistent with the ATL "hub" hypothesis.

4.4. Study Limitations

Although we systematically chose patient scans at the patient's earliest time point in a longitudinal study, we did not attempt to match cohorts relative to global atrophy or time post disease onset. As PPA is a neurodegenerative disease, the degree to which resting-state networks are compromised varies depending on the stage of disease progression. More closely matched cohorts would be helpful in order to understand variations in RSFC patterns between the three PPA variants relative to specific disease staging.

Longitudinal studies of lvPPA patients have revealed significant changes in both total gray matter loss and atrophy location over time (Rohrer et al., 2013). In order to assess alterations in RSFC above and beyond the effect of atrophy, we used gray matter as an imaging covariate in our ANCOVA model. We saw substantially more right hemisphere network dysfunction in RSFC compared to controls, despite left-lateralized atrophy. More notably, group level differences were absent in areas where there was connectivity in control maps but not in RSFC networks for patients. Although the lack of significance at the group level may be a result of statistical thresholds in the one-sample *t*-test ($p<0.005$ FWE), other factors may have impacted the results. Atrophy, and therefore RSFC, can differ significantly between patients of the same variant. High variability in left hemisphere RSFC within each patient group may have impacted the

ANCOVA statistical model, minimizing statistically significant results within the left hemisphere, specifically. Given the prominent language deficits in PPA and left-lateralized atrophy (Gorno-Tempini et al., 2011), it is unlikely that RSFC is not substantially altered in the left hemisphere relative to controls. We hypothesize that prominent right hemisphere network-level dysfunction may be an artifact of the statistical model and a function of left greater-than right hemisphere RSFC variability in patients. Visual inspection of patient versus controls one-sample seed maps shows that RSFC networks for PPA are substantially different than controls. As such, our statistics likely did not capture the extent of network-wide dysfunction within the left hemisphere for PPA, as compared to controls, as a result of variability in both gray matter volume and RSFC. The ANCOVA statistical model with gray matter volumes as an imaging covariate may not be the best approach for group-level comparisons of RSFC in PPA versus controls.

4.5. Next Steps

Our next step will be to assess whether RSFC variability in PPA minimized significant results in the left hemisphere. To do so, we will examine mean signal and its standard deviation for areas which were statistically significant at $p<0.005$ FWE for controls, but not for PPA, and which did not survive the two-group comparison. Differences in the standard deviation for right versus left regions of interest will be informative about RSFC variability between hemispheres. Such results can help to guide future statistical analysis.

We would also like to explore RSFC networks within different ROIs. Given the significant group differences in the right hemisphere within left-seeded RSFC networks, homologous right hemisphere seeded networks may provide interesting additional information, as the left and right hemisphere appear to have differential functions in speech and language processing (Hurley et al., 2015; Vigneau et al., 2011). We would also like to investigate RSFC networks using different peak coordinates within our current broad regions of interest. A more refined ROI-seeded analysis based on subregions in the IFG could provide valuable information about dorsal and ventral language pathways. For example, subanatomical regions of the IFG are thought to have differential functions for semantics versus syntax (Liakakis et al., 2011). Furthermore, we could correlate RSFC to semantic and syntactic language performance on assessment tasks. Using ICA, amplitude of spontaneous low-frequency fluctuation (ALFF) in a regional STG-based RSFC network has been shown to positively predict performance in healthy subjects on a sound-to-word learning tasks, whereas ALFF in the default mode network negatively correlated with learning performance (Deng, Chandrasekaran, Wang, & Wong, 2015). Future research could analyze ALFF within our existing ROIs and correlate results with behavioral measures of motor-speech, syntax, phonology and semantic processing. Of particular interest would be the relationship between ALFF and nonword, irregular and regular word spelling and reading performance within ATL/SPT-seeded RSFC networks. Successful decoding of nonwords and irregular words requires selective recruitment of phonological and semantic processing, which could produce

differential ALFF scores within select variants of PPA (Henry et al., 2016; Sepelyak et al., 2011).

Relative to our results, it is possible that ROIs directly within atrophic areas contributed differentially to altered patterns of connectivity. Future analysis should examine the effects of placing ROIs within or very close to regions of atrophy. Such an analysis may be interesting in the context of graph theory. Future research could examine the implications of an atrophic ROI on the global efficiency, characteristic path length, and assortativity of the language network within PPA, as well as on the overall number of graphical nodes within the seed-based network. To standardize results among variants, researchers should attempt to match groups for total gray matter volume, as an indicator of atrophy.

In conclusion, this is the first study, to our knowledge, to examine RSFC in key nodes of the language network within all three variants of PPA. We demonstrated unique patterns of structural variance and RSFC networks in PPA. We confirmed predictions that RSFC networks would be significantly altered relative to controls and showed distinct patterns among the variants. Our results leave us with many unanswered questions that suggest new directions for future research. This study represents a critical first step toward exploring resting-state functional connectivity as a marker of disease state in patients with neurodegenerative disease.

Appendix

Table A1: Anatomical Abbreviations

Anatomical Region	Abbreviation
Amygdala	AMG
Angular Gyrus	ANG
Anterior Cingulate	ANT CING
Calcarine Gyrus	CALC
Caudate	CAUD
Cerebellum	CER
Cuneus	CUN
Fusiform Gyrus	FUS
Gyrus Rectus	RECT
Hescl's Gyrus	HESCL
Hippocampus	HIPP
Inferior Frontal Operculum	IFO
Inferior Parietal Lobe	IPL
Inferior Temporal Gyrus	ITG
Insula	INS
Lingual Gyrus	LG
Medial Superior Frontal Gyrus	MED SFG
Middle Cingulate	MID CING
Middle Frontal Gyrus	MFG
Middle Temporal Gyrus	MTG
Occipital Lobe	OL
Operculum	OPER
Orbitalfrontal Cortex	OFC
Pallidum	PALL
Paracentral Lobule	PCL
Parahippocampus Gyrus	PHG
Postcentral Gyrus	POSTC
Posterior Cinguate	POST CING
Precentral Gyrus	PREC
Precuneus	PRECU
Putamen	PUT
Superior Frontal Gyrus	SFG
Superior Parietal Lobe	SPL
Superior Temporal Gyrus	STG

Table A1 continued…

Supplementary Motor Area	SMA
Temporal Pole	TP
Thalamus	THAL

APPENDIX TABLES: CONTROLS

Table A2: Significant Clusters and Corresponding Anatomical Regions for IFG-Seeded RSFC Networks in Controls

Cluster (in voxel)	T Value	x,y,z (MNI)	Regions
38261	35.22	-40 20 20	L IFG
	21.91	-44 30 20	L IFG
	19.91	-48 22 22	L IFG
367	12.59	-14 6 6	L PALL
	10.73	-14 4 16	L CAUD
	8.23	-22 -2 10	L PUT
281	11.49	14 6 2	R PALL
	9.83	22 6 10	R PUT
	8.55	16 2 18	R CAUD
113	9.82	-14 30 -18	L OFC
	8.82	-8 40 -16	L RECT
	8.15	-12 46 -22	L OFC
159	9.77	62 -38 -10	R MTG
	8.27	62 -42 -2	R MTG
	7.89	56 -42 -14	R ITG
124	9.49	-10 -78 -18	L CER
	8.56	-2 -74 -20	L CER
	7.14	-10 -74 -10	L LG

Anatomical regions within significant clusters consist of 3 local maxima more than 8 mm apart. Analyses were corrected for multiple comparisons at the cluster level using family-wise error correction (FWE), $p<0.005$, with extent threshold of 30 voxels.

Table A3: Significant Clusters and Corresponding Anatomical Regions for SPT-Seeded RSFC Networks in Controls

Cluster (in voxel)	T Value	x,y,z (MNI)	Regions
58777	35.5	-58 -38 14	L STG

Table A3 continued…

	21.74	-50 -36 8	L MTG
	17.08	-54 2 -2	L STG
103	10.4	16 -28 -2	R THAL
	8.26	14 -22 6	R THAL
	7.94	20 -28 6	R THAL
171	9.17	-32 -12 -26	L FUS
	8.07	-30 -2 -26	L AMG
	7.63	-32 -20 -18	L HIPP
139	8.82	30 42 30	R MFG
	8.1	26 48 20	R SFG
	8.05	34 50 24	R MFG

Anatomical regions within significant clusters consist of 3 local maxima more than 8 mm apart. Analyses were corrected for multiple comparisons at the cluster level using family-wise error correction (FWE), $p<0.005$, with extent threshold of 30 voxels.

Table A4: Significant Clusters and Corresponding Anatomical Regions for ATL-Seeded RSFC Networks in Controls

Cluster (in voxel)	T Value	x,y,z (MNI)	Regions
5952	32.98	-50 6 -40	L ITG
	13.55	56 -6 -28	R ITG
	13.46	-62 -28 -6	L MTG
5053	12.64	2 -90 -6	L CALC
	12.31	-8 -46 34	L MID CING
	11.65	-50 -70 -8	L OL
3514	11.62	50 28 -4	R OFC
	11.56	62 -6 6	R HESCL
	11.29	50 -16 -16	R MTG
104	11.16	-10 30 56	L MED SFG
	8.9	-8 18 54	L SMA
	7.79	-12 38 52	L SFG
463	10.49	0 58 -22	L RECT
	9.45	-4 58 -8	L OFC
	8.95	-8 58 -20	L OFC
763	10.35	-10 60 30	L MED SFG
	9.8	-4 56 20	L MED SFG
	8.9	8 48 24	R ANT CING
326	10.16	24 -78 -30	R CER
	8.38	20 -86 -28	R CER

Table A4 continued…

	8.18	36 -82 -30	R CER
102	9.88	4 -24 72	R PCL
	7.9	6 -18 78	R SMA
465	9.46	50 -62 -20	R ITG
	9.12	42 -80 -6	R OL
155	9.15	-20 -78 -32	L CER
	8.35	-28 -86 -32	L CER

Anatomical regions within significant clusters consist of 3 local maxima more than 8 mm apart. Analyses were corrected for multiple comparisons at the cluster level using family-wise error correction (FWE), $p<0.005$, with extent threshold of 30 voxels.

APPENDIX TABLES: NON-FLUENT VARIANT PPA (NFVPPA)

Table A5: Significant Clusters and Corresponding Anatomical Regions for nfvPPA Voxel-Based Morphometry (VBM) Results

Cluster (in voxel)	T Value	x,y,z (MNI)	Regions
2823	8.97	-34 12 6	L INS
	8.14	-34 20 4	L INS
	7.9	-46 2 38	L PREC
285	8.94	-26 -10 56	L PREC
	6.81	-20 -10 64	L SFG
	6.23	-38 -4 54	L PREC
400	7.85	-6 8 50	L SMA
	6.59	-4 -6 46	L MID CING
	6.47	-6 -16 44	L MID CING
160	7.48	26 -4 54	R SFG
	6.36	40 0 48	R PREC
	5.79	38 -4 58	R MFG
295	7.41	-48 -14 44	L POSTC
	7.22	-52 -10 38	L POSTC
	6.1	-56 -6 24	L POSTC
378	7.34	36 24 0	R INS
	6.72	40 4 8	R INS
	6.65	38 -8 12	R INS
396	7.26	0 -22 4	R THAL
	6.46	-12 -14 10	L THAL
133	7.19	20 2 6	R PALL
141	7.1	52 -8 40	R PREC

Table A5 continued…

	7.04	44 -14 40	R PREC
	5.39	42 -16 52	R PREC

Anatomical regions within significant clusters consist of 3 local maxima more than 8 mm apart. Analyses were corrected for multiple comparisons at the cluster level using family wise error correction (FWE), $p<0.005$, with extent threshold of 50 voxels.

Table A6: Significant Clusters and Corresponding Anatomical Regions for IFG-Seeded RSFC Networks in nfvPPA

Cluster (in voxel)	T Value	x,y,z (MNI)	Regions
9200	31.18	-40 20 20	L IFG
	18.78	-50 22 20	L IFG
	14.52	-48 16 34	L IFO
1101	12.54	50 26 22	R IFG
	11.02	46 32 12	R IFG
	10.01	42 12 40	R MFG
188	10.93	-26 -94 -12	L OL
	8.81	-32 -82 -10	L OL
	8.69	-20 -96 -6	L OL
431	10.79	-30 -70 38	L OL
	10.02	-46 -54 32	L ANG
	9.16	-40 -64 38	L ANG
117	10.61	-4 42 -8	L OFC
	7.82	-2 36 -16	L RECT
622	10.44	-4 -46 46	L PRECU
	9.77	-4 -48 24	L POST CING
	9.09	8 -50 36	R MID CING
154	9.98	34 -66 40	R OL
	9.17	42 -56 44	R IPL
114	9.36	18 -96 2	R CALC
	8.45	22 -94 16	R OL

Anatomical regions within significant clusters consist of 3 local maxima more than 8 mm apart. Analyses were corrected for multiple comparisons at the cluster level using family-wise error correction (FWE), $p<0.005$, with extent threshold of 30 voxels.

Table A7: Significant Clusters and Corresponding Anatomical Regions for Group Differences between nfvPPA and Controls within IFG-Seeded RSFC Networks

Cluster (in voxel)	T Value	x,y,z (MNI)	Regions
259	6.08	26 -46 4	R PRECU
	3.97	16 -40 4	R PRECU
	3.95	32 -38 -2	R HIPP

Anatomical regions within significant clusters consist of 3 local maxima more than 8 mm apart. Analyses was calculated using a statistical threshold of $p<0.005$ (uncorrected), with an extent threshold of 30 voxels.

Table A8: Significant Clusters and Corresponding Anatomical Regions for SPT-Seeded RSFC Networks in nfvPPA

Cluster (in voxel)	T Value	x,y,z (MNI)	Regions
10939	31.94	-54 -40 14	L STG
	16.36	-52 -8 2	L STG
	13.72	-56 -28 12	L STG
2287	13.59	52 -36 14	R STG
	12.36	62 -42 12	R STG
	11.49	58 8 14	R OPER
159	9.93	-24 -60 50	L SPL
	9.23	-28 -44 36	L IPL
	8.92	-34 -50 48	L IPL
273	9.6	32 -76 -10	R FUS
	9.34	46 -68 -2	R MTG
	8.89	40 -74 -2	R OL
102	9.31	20 -48 54	R SPL
	9.22	30 -56 48	R SPL
	9.02	24 -44 62	R POSTC
219	9.24	-6 -44 66	L PRECU
	8.82	-6 -38 58	L PRECU
	8.77	-6 -36 74	L PCL

Anatomical regions within significant clusters consist of 3 local maxima more than 8 mm apart. Analyses were corrected for multiple comparisons at the cluster level using family-wise error correction (FWE), $p<0.005$, with extent threshold of 30 voxels.

Table A9: Significant Clusters and Corresponding Anatomical Regions for Group Differences between nfvPPA and Controls within SPT-Seeded RSFC Networks

Cluster (in voxel)	T Value	x,y,z (MNI)	Regions
137	5.13	4 8 8	R CAUD
	3.8	-8 6 6	L CAUD
154	4.22	-6 8 34	L MID CING
	3.4	-2 16 30	L ANT CING
	3.09	4 14 40	R MID CING
116	4.2	26 -78 -2	R FUS
	3.4	32 -86 -4	R OL

Anatomical regions within significant clusters consist of 3 local maxima more than 8 mm apart. Analyses were calculated using a statistical threshold of $p<0.005$ (uncorrected), with an extent threshold of 30 voxels.

Table A10: Significant Clusters and Corresponding Anatomical Regions for ATL-Seeded RSFC Networks in nfvPPA

Cluster (in voxel)	T Value	x,y,z (MNI)	Regions
2363	32.38	-52 6 -40	L ITG
	18.45	-48 12 -36	L TP
	13.11	-50 16 -12	L TP
911	13.89	36 12 -40	R TP
	12.62	44 2 -40	R ITG
	11.08	44 22 -34	R TP
130	11.26	26 -88 -28	R CER
	9.6	24 -80 -24	R CER
	9.08	34 -78 -28	R CER
367	11.17	-6 46 -18	L RECT
	10.29	8 60 -14	R OFC
	10.27	-8 54 -16	L RECT

Anatomical regions within significant clusters consist of 3 local maxima more than 8 mm apart. Analyses were corrected for multiple comparisons at the cluster level using family-wise error correction (FWE), $p<0.005$, with extent threshold of 30 voxels.

Table A11: Significant Clusters and Corresponding Anatomical Regions for Group Differences between nfvPPA and Controls within ATL-Seeded RSFC Networks

Cluster (in voxel)	T Value	x,y,z (MNI)	Regions
99	4.37	62 -16 46	R POSTC

Anatomical regions within significant clusters consist of 3 local maxima more than 8 mm apart. Analyses was calculated using a statistical threshold of $p<0.005$ (uncorrected), with an extent threshold of 30 voxels.

APPENDIX TABLES: LOGOPENIC VARIANT PPA (LVPPA)

Table A12: Significant Clusters and Corresponding Anatomical Regions for lvPPA Voxel-Based Morphometry (VBM) Results

Cluster (in voxel)	T Value	x,y,z (MNI)	Regions
15187	14.16	-64 -24 -22	L ITG
	13.70	-60 -38 0	L MTG
	13.58	-66 -32 -18	L ITG
1350	9.34	56 -14 -12	R MTG
	8.63	56 -32 -2	R MTG
	8.59	60 -38 6	R MTG
751	8.99	-10 -16 10	L THAL
	8.28	-4 -8 4	L THAL
	7.80	-6 -30 6	L THAL
210	8.17	-46 8 28	L IFO
	7.65	-52 8 16	L IFO
	6.13	-46 2 34	L PREC
1152	7.95	-14 -64 22	L CUN
	7.85	-4 -44 36	L MID CING
	7.48	-6 -62 6	L LG
201	7.07	-26 56 -4	L OFC
	7.00	-12 54 -8	L MED SFG
	6.15	-34 54 -6	L OFC
117	6.57	36 22 4	R INS
	6.08	38 8 4	R IPL

Anatomical regions within significant clusters consist of 3 local maxima more than 8 mm apart. Analyses were corrected for multiple comparisons at the cluster level using family wise error correction (FWE), $p<0.005$, with extent threshold of 50 voxels.

Table A13: Significant Clusters and Corresponding Anatomical Regions for IFG-Seeded RSFC Networks in lvPPA

Cluster (in voxel)	T Value	x,y,z (MNI)	Regions
694	26.85	-40 20 20	L IFG
	18.15	-34 12 26	L IFG
	16.84	-38 12 18	L IFG
175	15.49	-42 14 38	L MFG
	13.18	-46 2 38	L PREC
	11.70	-36 4 38	L PREC
109	13.82	2 34 48	L MED SFG
	12.14	6 38 38	R MED SFG
	11.96	-4 32 54	L MED SFG

Anatomical regions within significant clusters consist of 3 local maxima more than 8 mm apart. Analyses were corrected for multiple comparisons at the cluster level using family-wise error correction (FWE), $p<0.005$, with extent threshold of 30 voxels.

Table A14: Significant Clusters and Corresponding Anatomical Regions for Group Differences between lvPPA and Controls within IFG-Seeded RSFC Networks

Cluster (in voxel)	T Value	x,y,z (MNI)	Regions
1202	6.07	26 -50 6	R CALC
	4.93	32 -50 -2	R FUS
	4.4	-2 -56 2	CER
5968	5.82	-28 -66 50	L SPL
	5.81	-20 -72 48	L SPL
	5.59	-10 -72 60	L PRECU
505	5.33	-22 -80 -12	L FUS
	4.22	-30 -74 -14	L FUS
	4.09	-44 -64 -12	L OL
520	5.09	64 -8 -28	R ITG
	4.12	52 12 -44	R ITG
	3.92	54 14 -36	R TP
990	5.07	46 -74 -40	R CER
	4.51	24 -80 -40	R CER

Table A14 continued…

	4.23	2 -72 -46	CER
273	4.96	-28 -52 -2	L LG
	4.19	-20 -46 2	L PRECU
	4	-24 -62 4	L CALC
142	4.61	36 -2 -44	R ITG
	4.13	46 -2 -50	R ITG
	3.29	34 10 -50	R ITG
548	4.53	58 -50 -42	R CER
	4.45	36 -38 -42	R CER
	4.37	22 -34 -48	CER
285	4.45	4 -64 24	R PRECU
	3.62	0 -54 30	L POST CING
	3.35	-8 -70 20	L CALC
331	4.34	-34 28 -28	L TP
	4.32	-48 22 -18	L TP
	4.02	-34 24 -42	L MTG
161	4.15	-70 -42 18	L STG
	4.14	-62 -46 20	L STG
	3.34	-70 -38 6	L MTG
126	4.14	42 22 -16	R OFC
	3.57	40 22 -8	R INS
	3.3	50 30 -18	R OFC
139	4.08	50 -32 -12	R MTG
	4	56 -42 -18	R ITG
	3.77	44 -40 -14	R ITG
107	3.86	-16 -32 -24	L CER
	3.72	-22 -12 -18	L HIPP
	3.64	-18 -24 -20	L PHG
167	3.57	-12 -102 -2	L CALC
	3.54	-4 -92 8	L CALC
	3.44	-18 -92 2	L OL

Anatomical regions within significant clusters consist of 3 local maxima more than 8 mm apart. Analyses was calculated using a statistical threshold of $p<0.005$ (uncorrected), with an extent threshold of 30 voxels.

Table A15: Significant Clusters and Corresponding Anatomical Regions for SPT-Seeded RSFC Networks in lvPPA

Cluster (in voxel)	T Value	x,y,z (MNI)	Regions
889	23.95	-54 -40 14	L STG
	14.18	-60 -48 12	L STG
	13.78	-46 -42 12	L STG

Anatomical regions within significant clusters consist of 3 local maxima more than 8 mm apart. Analyses were corrected for multiple comparisons at the cluster level using family-wise error correction (FWE), $p<0.005$, with extent threshold of 30 voxels.

Table A16: Significant Clusters and Corresponding Anatomical Regions for Group Differences between lvPPA and Controls within SPT-Seeded RSFC Networks

Cluster (in voxel)	T Value	x,y,z (MNI)	Regions
1468	5.91	32 -76 -16	R FUS
	5.89	36 -62 -16	R FUS
	4.62	20 -94 10	R CUN
6039	5.88	48 -2 50	R PREC
	5.78	46 -10 48	R PREC
	5.67	42 -22 50	R POSTC
114	5.13	4 6 10	R CAUD
	3.08	10 12 10	R CAUD
	3.04	-4 8 8	L CAUD
151	4.98	6 52 40	R MED SFG
	3.77	-2 48 48	L MED SFG
	3.58	16 44 50	R SFG
322	4.94	-26 -86 -12	L OL
	4.06	-34 -88 -12	L OL
	3.87	-20 -80 -12	L LG
126	4.8	-54 0 -6	L STG
	3.44	-52 2 6	L OPER
122	4.64	-26 38 44	L MFG
	3.18	-30 44 32	L MFG
790	4.62	22 -76 40	R OL
	4.58	30 -86 34	R OL
	4.2	22 -84 26	R OL
336	4.36	-10 68 12	L MED SFG
	4.22	-18 68 2	L SFG

Table A16 continued…

	3.63	-20 64 20	L SFG
115	4.24	50 36 20	R MFG
	4.01	44 36 12	R IFG
	3.46	50 42 12	R MFG
219	4.13	2 44 -6	R OFC
	4.12	-2 58 -6	L OFC
	3.53	-6 40 -4	L ANT CING
178	4.09	20 28 52	R SFG
	4.03	28 40 40	R MFG
	3.64	24 36 46	R SFG
156	4.09	2 -54 24	R PRECU
	4.01	-6 -42 36	L MID CING
	3.87	2 -58 16	R CALC

Anatomical regions within significant clusters consist of 3 local maxima more than 8 mm apart. Analyses was calculated using a statistical threshold of $p<0.005$ (uncorrected), with an extent threshold of 30 voxels.

Table A17: Significant Clusters and Corresponding Anatomical Regions for ATL-Seeded RSFC Networks in lvPPA

Cluster (in voxel)	T Value	x,y,z (MNI)	Regions
326	29.27	-50 6 -40	L ITG
	15.13	-42 4 -42	L ITG
	12.85	-56 2 -34	L MTG

Anatomical regions within significant clusters consist of 3 local maxima more than 8 mm apart. Analyses were corrected for multiple comparisons at the cluster level using family-wise error correction (FWE), $p<0.005$, with extent threshold of 30 voxels.

Table A18: Significant Clusters and Corresponding Anatomical Regions for Group Differences between lvPPA and Controls within ATL-Seeded RSFC Networks

Cluster (in voxel)	T Value	x,y,z (MNI)	Regions
1859	5.73	60 -8 -6	R STG
	5.35	60 -38 8	R STG
	4.54	52 6 -4	R STG
295	5.14	-38 -66 -14	L FUS
	4.66	-48 -72 -6	L OL

Table A18 continued…

	4.48	-36 -58 -12	L FUS
498	4.86	6 -24 72	R PCL
	4.49	4 -34 70	R PCL
	4.2	6 -48 64	R PRECU
143	4.72	-6 -56 4	L CALC
	4.03	-6 -64 10	L CALC
	3.5	-20 -56 6	L CALC
380	4.7	20 -58 16	R CALC
	3.9	26 -66 28	R OL
	3.9	30 -72 24	R OL
329	4.45	-34 -90 6	L OL
	4.12	-22 -86 22	L OL
	3.95	-36 -90 18	L OL
100	4.34	24 -54 -14	R FUS
	3.91	26 -46 -8	R LG
218	4.31	-48 -14 14	L OPER
	4.18	-50 2 16	L PREC
	3.94	-52 -12 4	L STG
266	4.22	-66 -28 0	L MTG
	3.96	-64 -38 4	L MTG
	3.82	-66 -18 -2	L MTG
212	4.18	48 10 -24	R TP
	4.11	36 20 -14	R INS
	3.78	46 18 -24	R TP
451	4.15	6 -8 74	R SMA
	4.13	-22 -10 62	L SFG
	4.05	-4 -14 64	L SMA
190	4.15	58 -12 40	R POSTC
	3.84	58 -20 44	R POSTC
	3.4	44 -10 40	R PREC
110	4.05	22 -74 38	L OL
	3.08	12 -82 32	R CUN
215	3.94	28 -44 46	R POSTC
	3.92	30 -44 62	R POSTC
	3.85	26 -52 62	R SPL

Anatomical regions within significant clusters consist of 3 local maxima more than 8 mm apart. Analyses was calculated using a statistical threshold of $p<0.005$ (uncorrected), with an extent threshold of 30 voxels.

APPENDIX TABLES: SEMANTIC VARIANT PPA (SVPPA)

Table A19: Significant Clusters and Corresponding Anatomical Regions for svPPA Voxel-Based Morphometry (VBM) Results

Cluster (in voxel)	T Value	x,y,z (MNI)	Regions
10815	19.28	-28 -8 -18	L HIPP
	16.95	-30 6 -28	L TP
	16.90	-42 0 -20	L TP
2875	10.53	32 12 -30	R TP
	10.08	32 12 -42	R TP
	9.81	40 8 -30	R TP

Anatomical regions within significant clusters consist of 3 local maxima more than 8 mm apart. Analyses were corrected for multiple comparisons at the cluster level using family wise error correction (FWE), $p<0.005$, with extent threshold of 50 voxels.

Table A20: Significant Clusters and Corresponding Anatomical Regions for IFG-Seeded RSFC Networks in svPPA

Cluster (in voxel)	T Value	x,y,z (MNI)	Regions
2490	31.58	-40 20 20	L IFG
	18.85	-44 26 28	L IFG
	14.9	-36 30 18	L IFG
448	13.47	-6 18 48	L SMA
	12.2	2 22 60	R SMA
	11.93	2 8 60	R SMA
303	13.43	52 24 26	R IFG
	11.63	38 32 32	R MFG
	11.37	36 22 26	R IFG
104	12.5	-6 -96 -2	L CALC
	9.47	-2 -94 6	L CALC
	9.37	-16 -94 -4	L CALC
366	11.99	-36 -54 38	L IPL
	10.55	-40 -58 46	L ANG
	10.12	-32 -68 48	L SPL

Anatomical regions within significant clusters consist of 3 local maxima more than 8 mm apart. Analyses were corrected for multiple comparisons at the cluster level using family-wise error correction (FWE), $p<0.005$, with extent threshold of 30 voxels.

Table A21: Significant Clusters and Corresponding Anatomical Regions for Group Differences between svPPA and Controls within IFG-Seeded RSFC Networks

Cluster (in voxel)	T Value	x,y,z (MNI)	Regions
119	4.2	-32 -14 -38	L FUS
	4.0604	-26 -10 -46	L FUS
	3.0185	-26 -6 -38	L FUS

Anatomical regions within significant clusters consist of 3 local maxima more than 8 mm apart. Analyses was calculated using a statistical threshold of $p<0.005$ (uncorrected), with an extent threshold of 30 voxels.

Table A22: Significant Clusters and Corresponding Anatomical Regions for SPT-Seeded RSFC Networks in svPPA

Cluster (in voxel)	T Value	x,y,z (MNI)	Regions
9969	29.13	-54 -40 14	L STG
	19.38	-58 -32 14	L STG
	17.64	-18 -78 -10	L LG
763	18.43	6 -12 46	R MID CING
	15.72	10 -28 48	R MID CING
	12.55	-2 -16 54	L SMA
1861	16.26	56 -2 14	R OPER
	16.18	44 -24 8	R HESCL
	15.75	60 0 6	R OPER
223	14.13	54 34 2	R IFG
	13.72	52 26 6	R IFG
	10.14	52 26 -4	R OFC
133	13.64	-26 -22 70	L PREC
	10.72	-18 -24 66	L PCL
	10.23	-32 -32 66	L POSTC
647	13.09	24 -36 56	R POSTC
	12.7	14 -46 68	R POSTC
	12	6 -38 76	R PCL
116	12.8	36 8 4	R INS
	11.7	30 2 -4	R PUT
	9.35	20 8 0	R PALL
121	11.83	-32 -46 54	L IPL
	11.48	-24 -54 56	L SPL
	10.24	-30 -60 58	L SPL
141	10.59	-50 18 -2	L IFG

Table A22 continued…

	10.54	-34 26 -10	L OFC
	10.4	-40 24 -2	L IFG

Anatomical regions within significant clusters consist of 3 local maxima more than 8 mm apart. Analyses were corrected for multiple comparisons at the cluster level using family-wise error correction (FWE), $p<0.005$, with extent threshold of 30 voxels.

Table A23: Significant Clusters and Corresponding Anatomical Regions for Group Differences between svPPA and Controls within SPT-Seeded RSFC Networks

Cluster (in voxel)	T Value	x,y,z (MNI)	Regions
154	4.8367	-40 -20 -32	L ITG
	4.5577	-32 -10 -30	L FUS
	4.4096	-40 -26 -26	L ITG
231	4.6621	-34 20 -28	L TP
	4.399	-32 6 -32	L TP
	3.9427	-26 6 -38	L TP
385	-4.4846	-36 -54 -6	L FUS
	-4.4517	-28 -54 12	L CALC
	-4.0557	-32 -64 -2	L LG
231	2.6674	-28 8 -36	L TP

Anatomical regions within significant clusters consist of 3 local maxima more than 8 mm apart. Analyses was calculated using a statistical threshold of $p<0.005$ (uncorrected), with an extent threshold of 30 voxels.

Table A24: Significant Clusters and Corresponding Anatomical Regions for ATL-Seeded RSFC Networks in svPPA

Cluster (in voxel)	T Value	x,y,z (MNI)	Regions
267	21.53	-50 6 -40	L ITG
	12.21	-50 12 -32	L TP
	8.72	-40 16 -42	L TP

Anatomical regions within significant clusters consist of 3 local maxima more than 8 mm apart. Analyses were corrected for multiple comparisons at the cluster level using family-wise error correction (FWE), $p<0.005$, with extent threshold of 30 voxels.

Table A25: Significant Clusters and Corresponding Anatomical Regions for Group Differences between svPPA and Controls within ATL-Seeded RSFC Networks

Cluster (in voxel)	T Value	x,y,z (MNI)	Regions
523	5.9254	12 -90 -2	R CALC
	4.052	20 -80 16	R CALC
	3.8802	24 -94 10	R OL
592	5.5363	-50 26 16	L IFG
	4.9278	-40 30 -10	L OFC
	4.5581	-34 30 8	L IFG
101	5.2057	-6 22 52	L SMA
	3.4622	-6 12 54	L SMA
	2.9319	-8 6 64	L SMA
163	5.0683	60 -40 6	R MTG
	3.3906	66 -32 6	R STG
	3.3054	60 -50 12	R MTG
109	5.0573	-60 -18 -4	L MTG
	3.8029	-58 -10 -6	L MTG
425	4.9862	18 -62 2	R LG
	4.0833	12 -66 12	R CALC
	3.8719	14 -42 6	R PREC
404	4.8463	-6 44 20	L MED SFG
	4.4245	-4 50 26	L MED SFG
	3.8521	-4 48 36	L MED SFG
498	4.7383	-58 -56 18	L MTG
	4.5056	-64 -40 12	L STG
	4.4465	-58 -40 6	L MTG
100	4.5794	50 36 12	R IFG
	3.6684	50 24 6	R IFG
	2.9852	48 42 2	R IFG
199	4.4891	-58 -8 12	L OPER
	3.8184	-60 -18 10	L STG
	3.4949	-54 -16 4	L STG
171	4.4242	-18 -50 -10	L LG
	4.0107	-16 -54 0	L LG
	3.6405	-12 -50 10	L PREC
230	4.4058	-20 -76 34	L OL
	3.872	-4 -78 4	L LG
	3.7745	-8 -78 12	L CALC
162	4.3874	6 -16 44	R MID CING
	3.9014	12 -12 40	R MID CING

Table A25 continued…

	3.5015	-10 -14 42	L MID CING
126	4.2928	36 -16 0	R PUT
	3.8664	34 -12 -10	R HIPP
	3.8181	20 -22 -2	R THAL
443	4.2162	48 -18 42	R PREC
	4.2093	34 -32 36	R POSTC
	4.143	52 -10 62	R PREC
109	4.2139	10 -12 72	R SMA
	3.5645	10 0 72	R SMA
	2.9742	20 -16 72	R SFG
203	4.1159	-56 -16 44	L POSTC
	3.8245	-54 -14 34	L POSTC
	3.6624	-50 -24 46	L POSTC
125	4.0922	-36 -62 -12	L FUS
	4.0657	-46 -76 -14	L OL
	3.1647	-46 -82 -6	L OL
188	4.0644	38 -60 -48	R CER
	3.9767	30 -58 -48	R CER
	3.7396	42 -70 -46	R CER
152	4.0269	38 24 -18	R OFC
	3.9967	30 18 -30	R TP
	3.2888	26 22 -24	R OFC

Anatomical regions within significant clusters consist of 3 local maxima more than 8 mm apart. Analyses was calculated using a statistical threshold of $p<0.005$ (uncorrected), with an extent threshold of 30 voxels.

References

Acosta-Cabronero, J., Patterson, K., Fryer, T., Hodges, J., Pengas, G., Williams, G., & Nestor, P. (2011). Atrophy, hypometabolism and white matter abnormalities in semantic dementia tell a coherent story. *Brain, 134*(7), 2025-2035.

Agosta, F., Sala, S., Valsasina, P., Meani, A., Canu, E., Magnani, G.,… & Filippi, M. (2013). Brain network connectivity assessed using graph theory in frontotemporal dementia. *Neurology, 81*(2), 134-143.

Ashburner, J. (2007). A fast diffeomorphic image registration algorithm. *Neuroimage, 38*(1), 95–113.

Baddeley, A. (2003). Working memory: Looking back and looking forward. *Nature Reviews Neuroscience*, *4*(10), 829-839.

Beckmann, C., DeLuca, M., Devlin, J., & Smith, S. (2005). Investigations into resting-state connectivity using independent component analysis. *Philosophical Transactions of the Royal Society of Biological Sciences*, *360,* 1001–1013.

Binder, J., Desai, R., Graves, W., & Conant, L. (2009). Where is the semantic system? A critical review and meta-analysis of 120 functional neuroimaging studies. *Cerebral Cortex, 19*(12), 2767-2796.

Binney, R., Embleton, K., Jefferies, E., Parker, G. & Lambon Ralph, M. (2010). The ventral and inferolateral aspects of the anterior temporal lobe are crucial in semantic memory: Evidence from a novel direct comparison of distortion-corrected fMRI, rTMS, and semantic dementia. *Cerebral Cortex, 20,* 2728-2738.

Booth, J., Wood, L., Lu, D., Houk, J., & Bitan, T. (2007). The role of the basal ganglia and cerebellum in language processing. *Brain Research, 1133,* 136-144.

Bookheimer, S., Zeffiro, T., Blaxton, T., Gaillard, W., & Theodore, W. (2000). Activation of language cortex with automatic speech tasks. *Neurology, 55,* 1151 – 1157.

Buchsbaum, B., & D'Esposito, M. (2008). The search for the phonological store: From loop to convolution. *Journal of Cognitive Neuroscience, 20,* 762–778.

Buchsbaum, B., Hickok, G., & Humphries, C. (2001). Role of left posterior superior temporal gyrus in phonological processing for speech perception and production. *Cognitive Science, 25*(5), 663-678.

Buchsbaum, B., Baldo, J., Okada, K., Berman, K., Dronkers, N., D'Esposito, M., & Hickok, G. (2011). Conduction aphasia, sensory–motor integration, and phonological short-term memory: An aggregate analysis of lesion and fMRI data. *Brain and Language*, *119,* 119-128.

Buchsbaum, B., Olsen, R., Koch, P., & Berman, K. (2005a). Human dorsal and ventral auditory streams subserve rehearsal-based and echoic processes during verbal working memory. *Neuron, 48,* 687–697.

Buchsbaum, B., Olsen, R., Koch, P., Kohn, P., Kippenhan, J., & Berman, K. (2005b). Reading, hearing, and the planum temporale. *Neuroimage*, *24*, 444–454.

Callan, D., Tsytsarev, V., Hanakawa, T., Callan, A., Katsuhara, M., Fukuyama, H., & Turner, R. (2006). Song and speech: Brain regions involved with perception and covert production. *Neuroimage, 31,* 1327–1342.

Campanella, F., Fabbro, F., & Urgesi, C. (2013). Cognitive and anatomical underpinnings of the conceptual knowledge for common objects and familiar people: A repetitive transcranial magnetic stimulation study. *PLOS One*, *8,* e64596.

Casanova R., Srikanth R., Baer A., Laurienti P., Burdette J., Hayasaka S… & Maldjian, J. (2007). Biological parametric mapping: A statistical toolbox for multimodality brain image analysis. *NeuroImage*, *34*(1), 137-143.

Champod, A., & Petrides, M. (2010). Dissociation within the frontoparietal network in verbal working memory: A parametric functional magnetic resonance imaging study. *The Journal of Neuroscience, 30*(10), 3849-3856.

Chein, J., Fissell, K., Jacobs, S., & Fiez, J. (2002). Functional heterogeneity within Broca's area during verbal working memory. *Physiology and Behavior*, *77,* 635-639.

Clerget, E., Poncin, W., Fadiga, L. & Olivier, E. (2012). Role of Broca's area in implicit motor skill learning: Evidence from continuous theta-burst magnetic stimulation. *Journal of Cognitive Neuroscience, 24*(1), 80–92.

Day, G., Farb, N., Tang-Wai, D., Masellis, M., Black, S., Freedman, M., ... & Chow, T. (2013). Salience network resting-state activity: Prediction of frontotemporal dementia progression. *JAMA Neurology, 70*(10), 1249-1253.

Deng, Z., Chandrasekaran, B., Wang, S., & Wong, P. (2015). Resting-state low-frequency fluctuations reflect individual differences in spoken language learning. *Cortex*, *76,* 63-78.

Du Boisgueheneuc, F., Levy, R., Volle, E., Seassau, M., Duffau, H., Kinkingnehun, S., ... & Dubois, B. (2006). Functions of the left superior frontal gyrus in humans: A lesion study. *Brain*, *129*(12), 3315-3328.

Farb, N., Grady, C., Strother, S., Tang-Wai, D., Masellis, M., Black, S., … & Chow, T. (2013). Abnormal network connectivity in frontotemporal dementia: Evidence for prefrontal isolation. *Cortex*, *49,* 1856-1873.

Fiez, J., Tranel, D., Seager-Frerichs, D., & Damasio, H. (2006). Specific reading and phonological processing deficits are associated with damage to the left frontal operculum. *Cortex*, *42*(4), 624-643.

Filippi, M., Rocca, M. A., Barkhof, F., Brück, W., Chen, J. T., Comi, G., ... & Fazekas, F. (2012). Association between pathological and MRI findings in multiple sclerosis. *The Lancet Neurology, 11*(4), *349*-360.

Friederici, A., & Gierhan, S. (2013). The language network. *Current Opinions In Neurobiology, 23*(2), 250-254.

Friederici, A., Rüschemeyer, S., Hahne, A., & Fiebach, C. (2003). The role of left inferior frontal and superior temporal cortex in sentence comprehension: Localizing syntactic and semantic processes. *Cerebral Cortex*, *13*(2), 170-177.

Folstein, M., Folstein, S., & McHugh, P. (1975). "Mini-mental state": A practical method for grading the cognitive state of patients for the clinician. *Journal of Psychiatric Research*, *12*(3), 189-198.

Galantucci, S., Tartaglia, M., Wilson, S., Henry, M., Filippi, M., Agosta, F., ... & Gorno-Tempini, M. (2011). White matter damage in primary progressive aphasias: A diffusion tensor tractography study. *Brain,* awr099.

Galton C., Patterson K., Graham K., Lambon-Ralph M., Williams G., Antoun N. … & Hodges J. (2001). Differing patterns of temporal atrophy in Alzheimer's disease and semantic dementia. *Neurology, 57,* 216--225.

Goldberg, G. (1985). Supplementary motor area structure and function: Review and hypotheses. *Behavioral and Brain Sciences, 8*(04), 567-588.

Gorno-Tempini, M., Brambati, S., Ginex, V., Ogar, J., Dronkers, N., Marcone, A., ... & Miller, B. (2008). The logopenic/phonological variant of primary progressive aphasia. *Neurology, 71*(16), 1227-1234.

Gorno-Tempini, M., Dronkers, N., Rankin, K., Ogar, J., Phengrasamy, L., Rosen, … & Miller, B. (2004). Cognition and anatomy in three variants of primary progressive aphasia. *Annals of Neurology, 55,* 335-346.

Gorno-Tempini, M., Hillis, A., Weintraub, S., Kertesz, A., Mendez, M., Cappa, & S., Grossman, M. (2011). Classification of primary progressive aphasia and its variants. *Neurology, 76,* 1006-1014.

Guo, C., Gorno-Tempini, M., Gesierich, B., Henry, M., Trujillo, A., Shany-Ur, T., … & Seeley, W. (2013). Anterior temporal lobe degeneration produces widespread network-driven dysfunction. *Brain, 136*, 2979-2991.

Hallquist, M., Hwang, K., & Luna, B. (2013). The nuisance of nuisance regression: spectral misspecification in a common approach to resting-state fMRI

preprocessing reintroduces noise and obscures functional connectivity. *Neuroimage, 82,* 208-225.

Henry, M., & Gorno-Tempini, M. (2010). The logopenic variant of primary progressive aphasia. *Current Opinions in Neurology, 23*(6), 633-637.

Henry, M., Wilson, S., Babiak, M., Mandelli, M., Beeson, P., Miller, Z., & Gorno-Tempini, M. (2016). Phonological processing in primary progressive aphasia. *Journal of Cognitive Neuroscience*. *28*(2), 210-222.

Hickok, G. (2014). The architecture of speech production and the role of the phoneme in speech processing. *Language, Cognition and Neuroscience, 29*(1), 2-20.

Hickok, G. (2012). The cortical organization of speech processing: Feedback control and predictive coding the context of a dual-stream model. *Journal of Communication disorders, 45*(6), 393-402.

Hickok, G., Buchsbaum, B., Humphries, C., & Muftuler, T. (2003). Auditory–motor interaction revealed by fMRI: speech, music and working memory in area Spt. *Journal of Cognitive Neuroscience, 15,* 673–682.

Hickok, G., Okada, K., & Serences, J. (2009). Area SPT in the human planum temporale supports sensory-motor integration for speech processing. *Journal of Neurophysiology, 101,* 2725-2732.

Hickok, G., & Poeppel, D., (2004). Dorsal and ventral streams: A framework for understanding aspects of the functional anatomy of language. *Cognition, 92,* 67-99.

Hickok, G., & Poeppel, G. (2007). The cortical organization of speech processing. *Nature Reviews, 8,* 393-402.

Hodges, J., & Patterson, K. (2007). Semantic dementia: A unique clinicopathological syndrome. *Lancet Neurology, 6,* 1004-1014.

Hurley, R., Bonakdarpour, B., Wang, X., & Mesulam, M. (2015). Asymmetric connectivity between the anterior temporal lobe and the language network. *Journal of Cognitive Neuroscience, 27*(3), 464-473.

Irish, M., Hodges, J. R., & Piguet, O. (2013). Episodic future thinking is impaired in the behavioural variant of frontotemporal dementia. *Cortex, 49*(9), 2377-2388.

Jackson, R., Hoffman, P., Pobric, G., & Ralph, M. (2016). The semantic network at work and rest: Differential connectivity of anterior temporal lobe subregions. *The Journal of Neuroscience, 36*(5), 1490-1501.

Jefferies, E. (2013). The neural basis of semantic cognition: Converging evidence from neuropsychology, neuroimaging and TMS. *Cortex, 49*(3), 611-625.

Jefferies E., Patterson K., Jones R., & Lambon Ralph, M. (2009). Comprehension of concrete and abstract words in semantic dementia. *Neuropsychology, 23*, 492—499.

Jobard, G., Crivello, F., & Tzourio-Mazoyer, N. (2003). Evaluation of the dual route theory of reading: A metanalysis of 35 neuroimaging studies. *Neuroimage*, *20*(2), 693-712.

Jones, D., Vemuri, P., Murphy, M., Gunter, J., Senjem, M., Machulda, M., ... & Boeve, B. (2012). Non-stationarity in the "resting brain's" modular architecture. *PloS One*, *7*(6), e39731.

Josephs, K., Duffy, J., Strand, E., Whitwell, J., Layton, K., Parisi, J., ... & Dickson, D. (2006). Clinicopathological and imaging correlates of progressive aphasia and apraxia of speech. *Brain, 129*(6), 1385-1398.

Kümmerer, D., Hartwigsen, G., Kellmeyer, P., Glauche, V., Mader, I., Klöppel, S., ... & Saur, D. (2013). Damage to ventral and dorsal language pathways in acute aphasia. *Brain, 136*(2), 619-629.

La Joie, R., Landeau, B., Perrotin, A., Bejanin, A., Egret, S., Pélerin, A., ... & Desgranges, B. (2014). Intrinsic connectivity identifies the hippocampus as a main crossroad between Alzheimer's and semantic dementia-targeted networks. *Neuron,* 81(6), 1417-1428.

Lambon Ralph, M. (2014). Neurocognitive insights on conceptual knowledge and its breakdown. *Philosophical Transactions of the Royal Society of London B: Biological Sciences, 369*(1634), 20120392.

Lambon Ralph M., Pobric G, & Jefferies E. (2009). Conceptual knowledge is underpinned by the temporal pole bilaterally: Convergent evidence from rTMS. *Cerebral Cortex*. *19,* 832--838.

Lambon Ralph, M., Sage, K., Jones, R., & Mayberry, E. (2010). Coherent concepts are computed in the anterior temporal lobes. *Proceedings of the National Academy of Sciences, 107*(6), 2717.

Lee, M., Smyser, C., & Shimony, J. (2013). Resting-state fMRI: A review of methods and clinical applications. *American Journal of Neuroradiology, 34*(10), 1866-1872.

Lehmann, M., Madison, C., Ghosh, P., Seeley, W., Mormino, E., Greicius, M.D., … & Rabinovici, G., (2013). Intrinsic connectivity networks in healthy subjects explain clinical variability in Alzheimer's disease. *Proceedings of the National Academy of Sciences of the USA, 110,* 11606-11611.

Lehmann, M., Madison, C., Ghosh, P., Miller, Z., Greicius, M., Kramer, J., … & Rabinovici, G. (2015). Loss of functional connectivity is greater outside the default mode network in nonfamilial early-onset Alzheimer's disease variants. *Neurobiology of Aging, 36*(10), 2678-2868.

Liakakis, G., Nickel, J., & Seitz, R. (2011). Diversity of the inferior frontal gyrus—a meta-analysis of neuroimaging studies. *Behavioural Brain Research, 225*(1), 341-347.

Mandelli, M.,Vilaplana, E.,Brown, J., Hubbard, I., Binney, R., … & Gorno-Tempini, M. (in press). Healthy brain connectivity predicts atrophy progression in nonfluent variant of primary progressive aphasia. *Brain*.

Madhavan, A., Whitwell, J., Weigand, S., Duffy, J., Strand, E., Machulda, M., ... & Petersen, R. (2013). FDG PET and MRI in logopenic primary progressive aphasia versus dementia of the Alzheimer's type. *PLoS One, 8*(4), e62471.

Mahoney, C., Malone, I., Ridgway, G., Buckley, A., Downey, L., Golden, H., ... & Fox, N. (2013). White matter tract signatures of the progressive aphasias. *Neurobiology of Aging, 34*(6), 1687-1699.

Morris, J. (1993). The Clinical Dementia Rating (*CDR*): Current vision and scoring rules. *Neurology*.

Mummery, C., Patterson, K., Price, C., Ashburner, J., Frackowiak, R., & Hodges, J. (2000). A voxel-based morphometry study of semantic dementia: relationship between temporal lobe atrophy and semantic memory. *Annals of Neurology, 47*(1), 36-45.

Noonan, K., Jefferies, E., Corbett, F., & Ralph, M. (2010). Elucidating the nature of deregulated semantic cognition in semantic aphasia: Evidence for the roles of prefrontal and temporo-parietal cortices. *Journal of Cognitive Neuroscience, 22*(7), 1597-1613.

Noonan, K., Jefferies, E., Visser, M., & Ralph, M. (2013). Going beyond inferior prefrontal involvement in semantic control: evidence for the additional contribution of dorsal angular gyrus and posterior middle temporal cortex. *Journal of Cognitive Neuroscience, 25*(11), 1824-1850.

Okada, K., & Hickok, G. (2006). Left posterior auditory-related cortices participate both in speech perception and speech production: Neural overlap revealed by fMRI. *Brain and Language, 98*(1), 112-117.

Okada, K., Smith, K., Humphries, C., & Hickok, G. (2003). Word length modulates neural activity in auditory cortex during covert object naming. *Neuroreport, 14,* 2323–2326.

Pa, J., & Hickok, G. (2008). A parietal–temporal sensory–motor integration area for the human vocal tract: Evidence from an fMRI study of skilled musicians. *Neuropsychologia, 46,* 362–368.

Patterson, K., Nestor, P., & Rogers, T. (2007). Where do you know what you know? The representation of semantic knowledge in the human brain. *Nature Reviews Neuroscience, 8*(12), 976-987.

Peelle, J., Troiani, V., Gee, J., Moore, P., McMillan, C., Vesely, L., & Grossman, M. (2008). Sentence comprehension and voxel-based morphometry in progressive nonfluent aphasia, semantic dementia, and nonaphasic frontotemporal dementia. *Journal of Neurolinguistics, 21*(5), 418-432.

Peschke, C., Ziegler, W., Eisenberger, J., & Baumgaertner, A. (2012). Phonological manipulation between speech perception and production activates a parieto-frontal circuit. *NeuroImage, 59,* 788-799.

Pievani, M., de Haan, W., Wu, T., Seeley, W., & Frisoni, G. (2011). Functional network disruption in the degenerative dementias. *The Lancet, 10*(9), 829-843.

Premi, E., Cauda, F., Gasparotti, R., Diano, M., Archetti, S., Padovani, A., & Borroni, B. (2014). Multimodal fMRI resting-state functional connectivity in Granulin Mutations: The case of fronto-parietal dementia. *PloS one, 9*(9), e106500.

Pobric G., Jefferies E., Lambon Ralph M. (2007). Anterior temporal lobes mediate semantic representation: Mimicking semantic dementia by using rTMS in normal participants. *Proceedings of the National Acadamy of Science U S A. 104,* 20137-20141.

Puce, A., Constable, R., Luby, M., McCarthy, G., Nobre, A., Spencer, D., ... & Allison, T. (1995). Functional magnetic resonance imaging of sensory and motor cortex: comparison with electrophysiological localization. *Journal of Neurosurgery, 83*(2), 262-270.

Ranasinghe, K., Hinkley, L., Beagle, A., Mizuiri, D., Dowling, A., Honma, S., … & Vossel, K. (2014). Regional functional connectivity predicts distinct cognitive impairments in Alzheimer's disease spectrum. Clinical *NeuroImage, 5,* 385-395.

Rauschecker, J., & Scott, S. (2009). Maps and streams in the auditory cortex: Nonhuman primates illuminate human speech processing. *Nature Neuroscience*, *12*(6), 718-724.

Rogers, T., Lambon Ralph, M., Garrard, P., Bozeat, S., McClelland, J., Hodges, J., & Patterson, K. (2004). Structure and deterioration of semantic memory: A neuropsychological and computational investigation. *Psychological Review, 111*(1), 205.

Rohrer, J., Caso, F., Mahoney, C., Henry, M., Rosen, H., Rabinovici, G., ... & Ridgway, G. (2013). Patterns of longitudinal brain atrophy in the logopenic variant of primary progressive aphasia. *Brain and Language, 127*(2), 121-126.

Rohrer, J., Ridgway, G., Crutch, S., Hailstone, J., Goll, J., Clarkson, M., ... & Warrington, E. (2010). Progressive logopenic/phonological aphasia: erosion of the language network. *Neuroimage, 49*(1), 984-993.

Rohrer, J., Warren, J., Modat, M., Ridgway, G., Douiri, A., Rossor, M., … & Fox, N. (2009). Patterns of cortical thinning in the language variants of frontotemporal lobar degeneration. *Neurology, 72,* 1562-1569.

Rogalski, E., Cobia, D., Harrison, T., Wieneke, C., Weintraub, S., & Mesulam, M. (2011). Progression of language decline and cortical atrophy in subtypes of primary progressive aphasia. *Neurology, 76*(21), 1804-1810.

Rogalski, E., Cobia, D., Martersteck, A., Rademaker, A., Wieneke, C., Weintraub, S., & Mesulam, M. (2014). Asymmetry of cortical decline in subtypes of primary progressive aphasia. *Neurology, 83*(13), 1184-1191.

Rosazza, C., Minati, L., Ghielmetti, F., Mandelli, M., & Bruzzone, M. (2012). Functional connectivity during resting-state functional MR imaging: Study of the correspondence between independent component analysis and region-of-interest-based methods. *American Journal of Neuroradiology, 33*, 180-187.

Rosen H., Kramer J., Gorno-Tempini M., Schuff N., Weiner M., & Miller, B. (2002). Patterns of cerebral atrophy in primary progressive aphasia. *American Journal of Geriatric Psychiatry, 10,* 89 –97.

Sakai, K., Kitaguchi, K. & Hikosaka, O. (2003). Chunking during human visuomotor sequence learning. *Experimental Brain Research, 152*(2), 229–242.

Satterthwaite, T., Elliott, M., Gerraty, R., Ruparel,, Loughead, J., Calkins, M., ... & Wolf, D. (2013). An improved framework for confound regression and filtering for control of motion artifact in the preprocessing of resting-state functional connectivity data. *Neuroimage, 64,* 240-256.

Schwindt, G., Graham, N., Rochon, E., Tang-Wai, D., Lobaugh, N., Chow, T., & Black, S. (2013). Whole-brain white matter disruption in semantic and nonfluent variants of primary progressive aphasia. *Human Brain Mapping, 34*(4), 973-984.

Seeley, W., Crawford, R., Zhou, J., Miller, B., & Greicius, M., (2009). Neurodegenerative diseases target large-scale human brain networks. *Neuron, 62,* 42-52.

Sepelyak, K., Crinion, J., Molitoris, J., Epstein-Peterson, Z., Bann, M., Davis, C., ... & Hillis, A. (2011). Patterns of breakdown in spelling in primary progressive aphasia. *Cortex, 47*(3), 342-352.

Smieskova, R., Allen, P., Simon, A., Aston, J., Bendfeldt, K., Drewe, J., ... & Scheffler, K. (2012). Different duration of at-risk mental state associated with neurofunctional abnormalities: A multimodal imaging study. *Human Brain Mapping, 33*(10), 2281-2294.

Sonty, S., Mesulam, M., Thompson, C., Johnson, N., Weintraub, S., Parrish, T., & Gitelman, D. (2003). Primary progressive aphasia: PPA and the language network. *Annals of Neurology, 53*(1), 35-49.

Tomasi, D., & Volkow, N. (2012). Resting functional connectivity of language networks: Characterization and reproducibility. *Molecular Psychiatry, 17,* 841-854.

Thompson-Schill, S., D'Esposito, M., & Kan, I. (1999). Double dissociation of frontal and temporal lobe contributions to semantic memory. *Journal of Cognitive Neuroscience*, 23-23.

Ueno, T., Saito, S., Rogers, T., & Ralph, M. (2011). Lichtheim 2: Synthesizing aphasia and the neural basis of language in a neurocomputational model of the dual dorsal-ventral language pathways. *Neuron, 72*(2), 385-396.

Verwey, W. (1996). Buffer loading and chunking in sequential keypressing. *Journal of Experimental Psychology, 22*(3), 544– 62.

Verwey, W. (2001). Concatenating familiar movement sequences: The versatile cognitive processor. *Acta Psychologica, 106,* 69–95.

Verwey, W. & Eikelboom, T. (2003). Evidence for lasting sequence segmentation in the discrete sequence-production task. *Journal of Motor Behavior, 35*(2), 171– 81.

Vigneau, M., Beaucousin, P., Herve, P., Duffau, H., Crivello, F., Houde, O., … & Tzourio-Mazoyer, N. (2006). Meta-analyzing left hemisphere language areas: Phonology, semantics, and sentence processing. *NeuroImage, 20,* 1414-1432.

Vigneau, M., Beaucousin, V., Hervé, P., Jobard, G., Petit, L., Crivello, F., ... & Tzourio-Mazoyer, N. (2011). What is right-hemisphere contribution to phonological, lexico-semantic, and sentence processing? Insights from a meta-analysis. *Neuroimage, 54*(1), 577-593.

Visser, M., & Lambon Ralph, M. (2011). Differential contributions of bilateral ventral anterior temporal lobe and left anterior superior temporal gyrus to semantic processes. *Journal of Cognitive Neuroscience, 23*(10), 3121-3131.

Wagner, A., Paré-Blagoev, E., Clark, J., & Poldrack, R. (2001). Recovering meaning: left prefrontal cortex guides controlled semantic retrieval. *Neuron, 31*(2), 329-338.

Whitwell, J., Jones, D., Duffy, J., Strand, E., Machulda, M., Przybelski, S., … & Josephs, K., (2015). Working memory and language network dysfunctions in logopenic aphasia: A task-free fMRI comparison with Alzheimer's dementia. *Neurobiology of Aging, 36,* 1245-1252.

Wilson, S., Galantucci, S., Tartaglia, M., & Gorno-Tempini, L., (2012). The neural basis of syntactic deficits in primary progressive aphasia. *Brain and Language, 122*(3), 190-198.

Wilson, S., & Iacoboni, M., (2006). Neural responses to non-native phonemes varying in producibility: Evidence for the sensorimotor nature of speech perception. *Neuro-image, 33,* 316–325.

Wymbs, N., Bassett, D., Mucha, P., Porter, M. & Grafton, S. (2012). Differential recruitment of the sensorimotor putamen and frontoparietal cortex during motor chunking in humans. *Neuron, 74*(5), 936–46.

Zenon, A., & Olivier, E. (2014). Contribution of the basal ganglia to spoken language: Is speech production like the other motor skills? *Behavioral and Brain Sciences, 37*(6), 576-576.

Zhou, J., Gennatas, E., Kramer, J., Miller, B., & Seeley, W. (2012). Predicting regional neurodegeneration from the healthy brain functional connectome. *Neuron, 73*(6), 1216-1227.

Zhou, J., Greicius, M., Gennatas, E., Growdon, M., Jang, J., Rabinovici, G., ... & Seeley, W. (2010). Divergent network connectivity changes in behavioural variant frontotemporal dementia and Alzheimer's disease. *Brain, 133*(5), 1352-1367.